Available online at www.sciencedirect.com

ScienceDirect

Advances in Space Research xxx (xxxx) xxx

ADVANCES IN SPACE RESEARCH (a COSPAR publication)

www.elsevier.com/locate/asr

Dynamics of a gyrostat satellite with the vector of gyrostatic moment tangent to the orbital plane

Renato H. Morais [a], Luís F.F.M. Santos [a,b], André R.R. Silva [a], Rui Melicio [c,d,*]

[a] LAETA-AEROG, Universidade da Beira Interior, Covilhã, Portugal
[b] ISEC Lisboa, Portugal
[c] LAETA-IDMEC, Instituto Superior Técnico, Universidade de Lisboa, Portugal
[d] ICT, Escola de Ciências e Tecnologia, Universidade de Évora, Évora, Portugal

Received 13 October 2021; received in revised form 17 February 2022; accepted 7 March 2022

Abstract

In this paper, a gyrostat satellite in a circular orbit with its gyrostatic moment tangent to the orbital plane and collinear with the orbital speed is studied regarding its equilibria, bifurcation of equilibria, and asymptotic stability conditions. In the general case, where any gyrostat angular momentum is aligned with any of the orbital coordinate frames, interesting results arose regarding its equilibria bifurcation regarding conditions near to the ones presented in this paper, namely equilibria regions outside their main regions near to the orbital plane tangent. For equilibria and bifurcation of equilibria, a symbolic-numerical method is used to obtain the polynomial equations in function of non-dimensional parameters whose roots are equivalent to the number of equilibria positions. For the asymptotic stability, the results are tested using the Lyapunov stability theory scheme.

Keywords: Aerospace dynamics; Satellite gyrostat; Equilibrium; Stabilisation; Bifurcation of equilibria

1. Introduction

Artificial satellites provide services vital for the global economy, like telecommunication and navigation. Space-based Earth observation and space monitoring are also intrinsic satellite usages and critical for understanding and addressing global challenges. The deployment of large constellations of satellites in low-Earth orbit, addressing the increasing need for the globalisation of affordable satellite coverage, has been underway and will be in the plans of several private companies for the next few years. This recent increase, and because the space sector is becoming very competitive, lead the sector to more effectiveness of space technology. So, companies that consider bigger lifespan, cheaper systems and enhanced capabilities are crucial to capture market share within the space sector, and to fulfil this, a deep understanding of satellite and orbital dynamics are required. It has long been recognised that introducing an angular momentum source into a satellite can be used to manipulate the equilibria and stability properties. Therefore, a gyrostat satellite can be modelled as a rigid body containing a source of constant angular momentum whose alignment changes based on the analysis. The satellite is in a circular orbit in a perfect inverse square law gravitational force field.

Longman (1968a) found all equilibrium orientations relative to gravitational torques for a gyrostat satellite whose internal angular momentum is along a principal axis of the body. For small enough angular momentums, twenty-four discrete equilibrium orientations were discovered, coincid-

* Corresponding author at: LAETA-IDMEC, Instituto Superior Técnico, Universidade de Lisboa, Portugal.
E-mail address: ruimelicio@gmail.com (R. Melicio).

https://doi.org/10.1016/j.asr.2022.03.004
0273-1177/

ing with the well-known 24 equilibria of a rigid body. As the angular momentum increases, these discrete solutions disappear, as groups of four, until the only solutions left are those which have the rotor axis aligned with the perpendicular to the orbital plane.

Longman (1968b), Longman and Roberson (1969) considered the design of satellite equilibria and stabilisation conditions using gravity gradient methods with the aid of angular momentum wheels. These studies also focus on the theoretical design tenets which influence the satellite equilibria and stability, considering the symmetric rotors change in direction and magnitude.

The behaviour of a special class of gyrostat configurations, which have the internal angular momentum vector lying in any plane formed by two principal axes of the satellite, was determined by Longman (1971). The author then studies its equilibria and stability, finding a new set of previously undescribed eight equilibrium orientations, together with two previously treated sets of eight orientations (Longman, 1968a), the maximum equilibrium orientations add-up to twenty-four.

Longman (1972) performed a stability analysis of all possible equilibria for gyrostat satellites under gravitational torques. It showed that, for the case where the axis of intermediate moment of inertia lies any place in the orbital plane, the found solutions form a boundary dividing those satellites that can be made Lyapunov stable from those that cannot. The division is influenced by choosing a sufficiently large component of internal angular momentum along the perpendicular to the orbital plane. Longman (1972) concluded that any configuration in the Lyapunov stable region can be considered in preliminary satellite design.

Longman (1973) noticed two families of equilibria for a given angular momentum, resulting in a tumbling motion. The stability of the tumbling motion was investigated, as well as the stability of the isolated equilibria. This motion was also studied by Kuang and Tan (2002), where a GPS-based attitude determination methodology was employed, resulting in the suppression of the gyrostat satellite tumbling motion with the proposed linear regulators.

The issue of passing from a gravity-gradient stabilised attitude to another equilibrium attitude by using a proper control of the rotors' angular speed is addressed by Anchev (1973), once again assuming a circular orbit, an inverse square gravitational field, and that the attitude of the satellite has no effect on the orbit.

Longman (1975) studied the conditions for which a satellite stabilised by the gravity gradient method, with constant angular momentum internal wheels, is designed to know all the earth pointing equilibrium orientations since the spacecraft may inadvertently acquire unfavourable orientations. The author also reviewed the literature containing solutions to various special cases of the finding equilibria problem. A method for ascertaining the equilibria and stability is given for the most general case, and a numerical example is exhibited using said method.

The hitherto studies assumed that the spinning symmetric rotors are perfectly maintained at constant speed. This idealisation is not always feasible and a more realistic approach is to consider that the rotor is regulated by a feedback control system. Therefore, Li and Longman (1982) studied the relationship between stability results using these idealised models and the stability results obtained using the more realistic feedback controlled rotor model for the full range of feedback gains.

The difficulty of finding attitude equilibria of the gyrostat with respect to the orbiting frame can be approached in two ways: (a) a direct method in which the gyrostat satellite with a specified relative angular momentum vector is given and the set of all possible equilibrium orientations is obtained; (b) an inverse method in which we choose the orientation of the satellite and then try to find the corresponding angular momentum vector that makes this orientation an equilibrium. Pascal and Stepanov (1991) selected a compromise between the two and performed a semi-inverse method in which some parameters giving the equilibrium orientation of the satellite and some components of the angular momentum vector are chosen arbitrarily, with the aim of finding new solutions to this method.

Since the turn of the century, the study of a gyrostat satellite dynamics on a circular orbit with constant angular momentum lied mainly on the influence of different orientations of the internal angular momentum vector on the satellite's stability and dynamics. Rubanovskii (1991) studied the bifurcation and stability for the case when the rotor axis does not lie in a system principal plane of inertia. Saryshev and Mirer (2001) found a new analytical solution of all equilibria for the case where the internal angular momentum of the gyrostat satellite is collinear to its principal axis of inertia. Following the 2001 study, Sarychev et al. (2005) determined the bifurcation values and showed the evolution of the regions of validity, for the same particular case, while Sarychev et al. (2008) studied the special case where the gyrostatic moment vector lies in one of the satellite's principal central planes of inertia. Molina and Mondéjar (2004) focused on the motion of a satellite that had, in the first case, spherical symmetry, and in the second case, axial symmetry. Shirazi and Ghaffari-Saadat (2005) considered the attitude dynamics of an asymmetrical gyrostat satellite, while Chaikin (2013) studied the case where the angular momentum aligns with the gyrostat principal central plane of inertia. Gutnik and Sarychev (2017) focused on the special case when the projection of the vector of gyrostatic torque is located in one of the principal central planes of inertia of the satellite.

The previous studies on the special cases of the angular momentum alignment improved the general case's common understanding and analysis. As such, the focus of determining the satellite's equilibrium orientation shifted to the case where the angular momentum is not aligned with any principal axis nor with the orbital coordinate frame. Sarychev et al. (2012) studied the equilibria of a gyrostat satellite and the number of solutions was proved

to be no less than 8 and no more than 24, as previously established. The following year, the stability conditions study led Sarychev et al. (2013) to perceive that the stable solutions decrease from 4 to 2 as the gyrostatic torque increases. Gutnik and Sarychev (2013), Gutnik and Sarychev (2014) adopted a different method which starts with the usage of an algorithm for the Groebner bases' construction and results in a conversion of the 9-equations/9-variables system into a 12th order algebraic equation with a single variable. Gutnik et al. (2015), Santos (2015) conducted a deep analysis of different equilibria and stability. Santos and Melicio (2020) described the number of equilibria orientations of the general case, when its angular momentum is not aligned with any principal axis of the satellite nor with any orbital coordinate frame. A complete numerical analysis was then performed to understand the evolution of the number of equilibria orientations. This analysis led to the detection of small equilibria regions when the vector of gyrostatic moment is tangent to the orbital plane. To confirm the existence of these regions, the current work intends to study this particular case, when the vector of gyrostatic moment is tangent to the orbital plane, to shed light on these solutions.

Other relevant studies have been researched, such as the dynamics of dual-spin spacecraft under effects of energy dissipation, where the damper masses in the platform and the rotor cause energy loss in the system (Nazari and Butcher, 2014), and the momentum transfer control of a torque-free gyrostat with a discrete damper, which uses an adaptive feedback linearisation method combined with neural networks (Seo et al., 2008). Zanardi and Moreira (2007) developed an analytical approach for the gyrostat attitude propagation using non-singular canonical variables to describe the rotational motion. Wang and Xu (2012) studied the relative equilibria of a rigid body, using geometric mechanics, when considering the J2 perturbations of an oblate gravitational field. Guirao and Vera (2010) analysed a gyrostat dynamics in the frame of the three-body problem using geometrical and mechanics methods to describe the Eulerian equilibria and to study their bifurcation, while Vera (2009) employed the same non-canonical Hamiltonian dynamics approach to the three-body problem for a triaxial gyrostat. Ousaloo (2016) developed a control scheme to overcome the nutation motion of an asymmetric satellite, independent of its inertia, by adding an axial reaction wheel on the desired spin axis. Aleksandrov et al. (2018) studied an electrodynamic attitude control system for a symmetric satellite on a circular orbit. Gorr (2021) proposed a new method for integrating the equations of motion reducing the original equation to a fifth-order system.

In the current paper, a gyrostat satellite with a particular configuration is studied. As mentioned above, a previous study Santos and Melicio, 2020, detected small equilibria regions when the gyrostatic moment of inertia is tangent to the orbital plane. The existence of these regions needs confirmation, as well as subsequent analysis of both the equilibria and stability of this case. In summation, the main contributions are: (i) development of an analytical method, which was numerically tested by software, to determine all the equilibrium and stability conditions for the configuration where the Satellite Vector of Gyrostatic Moment is Tangent to the Orbital Plane; (ii) the study of the equilibria evolution near when the angular momentum is aligned with the orbital tangent direction; (iii) analytically determination of the equilibrium bifurcation curves; (iv) analytically determination of the asymptotic stability evolution curves.

The paper is structured as follows: Section 2 explains the prototype design. Section 3 presents the prototype implementation. Section 4 focus on the experimental methods and results. Finally, Section 5 outlines conclusions.

2. Motion Equations

This section describes the equations of motion that rule a solid body with statically and dynamically balanced internal rotors. The rotor's angular velocity is assumed constant relative to the satellite's main body, while the satellite's centre of mass moves along a circular orbit in a central Newtonian gravitational field. Two right-handed Cartesian reference frames with origin at the satellite's centre of mass O are introduced. The first is the $OX_1X_2X_3$ which represents the orbital reference frame whose axis OX_3 is directed along the radius vector connecting the satellite's centre of mass and Earth's, the OX_1 axis is aligned with the linear velocity of the centre of mass O and the OX_2 is normal to the plane of orbit. The second cartesian reference is the $Ox_1x_2x_3$ which represents the satellite-fixed reference frame, where $Ox_i(i = 1, 2, 3)$ are the satellite's principal axes of inertia.

Let us define the orientation of the satellite-fixed reference frame relative to the orbital reference frame by the spacecraft angles α, β, and γ represented in Fig. 1, Where these Euler angles are a sequence of rotations of $Ox_1x_2x_3$

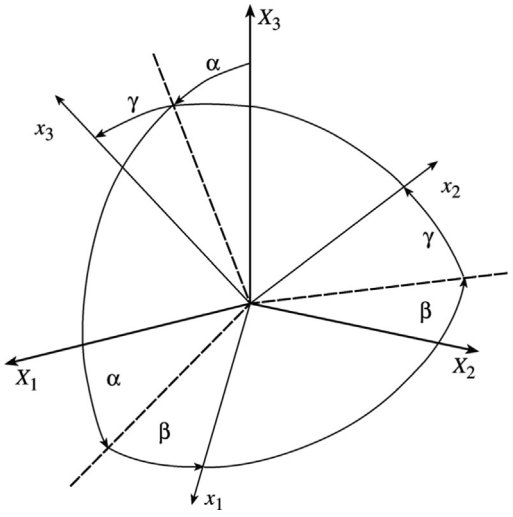

Fig. 1. Relation between Orbital and Gyrostat's reference frames Longman, 1972.

around the orbital reference system $OX_1X_2X_3$. Regarding this case study the chosen rotation sequence was the 2–3-1 (Kane and Ben-Asher, 1983) with α being the angle between OX_1X_3 (rotation of OX_2 axis), β being the angle between OX_1X_2 (rotation of OX_3 axis) and γ being the angle between OX_2X_3 (rotation of OX_1 axis). Consequently, the direction cosines $a_{ij} = cos(X_i, x_j)$ are specified by the following expressions (Sarychev et al., 2008):

$$\begin{cases} a_{11} = & \cos\alpha\cos\beta \\ a_{12} = & \sin\alpha\sin\gamma - \cos\alpha\sin\beta\sin\gamma \\ a_{13} = & \sin\alpha\cos\gamma + \cos\alpha\sin\beta\sin\gamma \\ a_{21} = & \sin\beta \\ a_{22} = & \cos\beta\cos\gamma \\ a_{23} = & -\cos\beta\sin\gamma \\ a_{31} = & -\sin\alpha\cos\beta \\ a_{32} = & \cos\alpha\sin\gamma + \sin\alpha\sin\beta\cos\gamma \\ a_{33} = & \cos\alpha\cos\gamma - \sin\alpha\sin\beta\sin\gamma \end{cases} \tag{1}$$

The equations governing the satellite attitude dynamics are written in the form (Saryshev and Mirer, 2001; Sarychev et al., 2008; Gutnik and Sarychev, 2017; Sarychev et al., 2013; Gutnik and Sarychev, 2013; Gutnik and Sarychev, 2014; Gutnik et al., 2015; Santos, 2015; Sarychev et al., 2012):

$$\begin{cases} A\dot{p} + (C-B)qr - 3\omega_0^2(C-B)a_{32}a_{33} - \overline{h_2}r + \overline{h_3}q = 0 \\ B\dot{q} + (A-C)rp - 3\omega_0^2(A-C)a_{33}a_{31} - \overline{h_3}p + \overline{h_1}r = 0 \\ C\dot{r} + (B-A)pq - 3\omega_0^2(B-A)a_{31}a_{32} - \overline{h_1}q + \overline{h_2}p = 0 \end{cases} \tag{2}$$

$$\begin{cases} p = (\dot{\alpha}+\omega_0)a_{21} + \dot{\gamma} = \overline{p} + \omega_0 a_{21} \\ q = (\dot{\alpha}+\omega_0)a_{22} + \dot{\beta}\sin\gamma = \overline{q} + \omega_0 a_{22} \\ r = (\dot{\alpha}+\omega_0)a_{23} + \dot{\beta}\cos\gamma = \overline{r} + \omega_0 a_{23} \end{cases} \tag{3}$$

Here, A, B, C are the gyrostat's principal central moments of inertia; p, q, r are the gyrostat's absolute angular velocity projections and $\overline{h_i}(i = 1, 2, 3)$ the gyrostatic angular moment vector projections onto axes Ox_i. Lastly, ω_0 is the orbital angular velocity of the gyrostat centre of mass, while the dots designate time differentiation.

3. Gyrostat's Equilibrium

Following (Sarychev et al., 2008), first, the designation $\overline{h_i}/\omega_0 = h_i$ is introduced and the ensuing system of equations are obtained:

$$\begin{cases} 4(A a_{21}a_{31} + B a_{22}a_{23} + C a_{23}a_{33}) \\ \qquad + h_1 a_{31} + h_2 a_{32} + h_3 a_{33} = 0 \\ A a_{11}a_{31} + B a_{12}a_{32} + C a_{13}a_{33} = 0 \\ A a_{11}a_{21} + B a_{12}a_{22} + h_1 a_{11} + h_2 a_{12} + h_3 a_{13} = 0 \end{cases} \tag{4}$$

This system allows the establishment of all gyrostat's equilibrium positions in the orbital reference frame. In this case, a_{ij}, as elements of an orthogonal matrix, satisfy the following conditions:

$$\begin{cases} a_{11}^2 + a_{12}^2 + a_{13}^2 = 1 \\ a_{21}^2 + a_{22}^2 + a_{23}^2 = 1 \\ a_{31}^2 + a_{32}^2 + a_{33}^2 = 1 \\ a_{11}a_{21} + a_{11}a_{21} + a_{11}a_{21} = 0 \\ a_{11}a_{31} + a_{12}a_{32} + a_{13}a_{33} = 0 \\ a_{21}a_{31} + a_{22}a_{32} + a_{23}a_{33} = 0 \end{cases} \tag{5}$$

At $A \neq B \neq C$ one can solve system (5) and (6) for $a_{11}, a_{12}, a_{13}, a_{21}, a_{22}, a_{23}$ and a_{23}.

$$\begin{cases} a_{11} = 4(C-B)a_{32}a_{33}/F \\ a_{12} = 4(A-C)a_{33}a_{31}/F \\ a_{13} = 4(B-A)a_{31}a_{33}/F \\ a_{21} = 4(I_3-A)a_{31}/F \\ a_{22} = 4(I_3-B)a_{32}/F \\ a_{23} = 4(I_3-C)a_{33}/F \end{cases} \tag{6}$$

Here, $F = h_1a_{31} + h_2a_{32} + h_3a_{33}, I_3 = Aa_{31}^2 + Ba_{32}^2 + Ca_{33}^2$, and direction cosines a_{31}, a_{32} and a_{33} are determined from the following:

$$\begin{cases} 16\Big[(B-C)^2a_{32}^2a_{33}^2 + (C-A)^2a_{33}^2a_{31}^2 + \\ +(A-B)^2a_{31}^2a_{32}^2\Big] = (h_1a_{31} + h_2a_{32} + h_3a_{33})^2 \\ 4(B-C)(C-A)(A-B)a_{31}a_{32}a_{33} + \\ [h_1(B-C)a_{32}a_{33} + h_2(C-A)a_{33}a_{31} + \\ +h_3(A-B)a_{31}a_{32}](h_1a_{31} + h_2a_{32} + h_3a_{33}) = 0 \\ a_{31}^2 + a_{32}^2 + a_{33}^2 = 1 \end{cases} \tag{7}$$

Solving system (7) will allow the computation of the direction cosine in (6). Note that solutions (6) only exist when, out of three direction cosines a_{31}, a_{32} and a_{33}, none two vanish simultaneously. The cases $a_{31} = a_{32} = 0, a_{32} = a_{33} = 0$ and $a_{33} = a_{31} = 0$ are special and should be considered immediately by addressing systems (4) and (5). The case $a_{32} = a_{33} = 0$ will be discussed later.

In previous studies, the general case of the gyrostat ($h_1 \neq 0, h_2 \neq 0$ and $h_3 \neq 0$) (Santos, 2015), as well as other particular cases, such as the case when the gyrostatic moment vector is collinear with one of the satellite's principal central axes of inertia ($h_1 = 0, h_2 \neq 0$ and $h_3 = 0$) (Saryshev and Mirer, 2001), and the case when the gyrostatic moment vector is parallel to the satellite's principal central plains of inertia ($h_1 = 0, h_2 = 0$ and $h_3 \neq 0$) (Sarychev et al., 2008) were analysed. In the present study, we deepen the knowledge on the case when the gyrostatic moment vector is along the satellite's local tangent with roll angle $\gamma = 0$, in which the parameter h_1 is zero ($h_1 = 0, h_2 \neq 0$ and $h_3 \neq 0$) which is not addressed within the current framework, particularly by Saryshev and Mirer (2001), Sarychev et al. (2008). The main objective of studying the case where $h_1 = 0$ is to assess the configurations of such gyrostat satellites, as well as verifying the

existence of small equilibrium regions out of their main region addressed in the General Case Bifurcation of Equilibria (Santos and Melicio, 2020).

Making $H_1 = 0$ and $H_2 = \frac{h_2}{C-A}, H_3 = \frac{h_3}{C-A}, v = \frac{A-B}{C-A}$, the system of 7 takes the form:

$$\begin{cases} 16\left[a_{32}^2 a_{33}^2 (v+1)^2 + a_{31}^2 a_{33}^2 + a_{32}^2 a_{33}^2 v^2\right] = \\ \qquad = (H_2 a_{32} + H_3 a_{33})^2 \\ a_{31}\{-4v(1+v) a_{32} a_{33} + [H_2 a_{33} + \\ \qquad + H_3 a_{32} v](H_2 a_{32} + H_3 a_{33})\} = 0 \\ a_{31}^2 + a_{32}^2 + a_{33}^2 = 1 \end{cases} \tag{8}$$

When investigating system (8) is clear that three different cases can exist. The first is $a_{31} \neq 0$ and $a_{32} = a_{33} = 0$, which solutions will be referred as Group I; the second case is when $a_{31} \neq 0, a_{32} \neq 0$ and $a_{33} \neq 0$, which solutions will be referred as Group II; and finally when $a_{31} = 0, a_{32} \neq 0$ and $a_{33} \neq 0$, which solutions will be referred as Group III.

For the case where $a_{31} \neq 0$ and $a_{32} = a_{33} = 0$, it is required to manipulate Eq. (8) to be dependent of a_{32} and a_{33} for assessing the solvability of (8):

$$\begin{cases} 16\left[a_{32}^2 a_{33}^2 + (v+1)^2 + a_{31}^2 a_{33}^2 + a_{32}^2 a_{33}^2 v^2\right] = \\ \qquad = (H_2 a_{32} + H_3 a_{33})^2 \\ -4v(1+v) a_{32} a_{33} + [H_2 a_{33} + \\ \qquad + H_3 a_{32} v](H_2 a_{32} + H_3 a_{33}) = 0 \\ a_{31}^2 + a_{32}^2 + a_{33}^2 = 1 \end{cases} \tag{9}$$

From the (9) it follows that, if $a_{32} = 0$, then $a_{33} = 0$. Eq. (9) gives no useful information since we fall into consistent dependent situation. To resolve this, the original Eqs. (4) and (5) need to be addressed, and develop this special case from there instead of (8). After manipulating (4) and (5), the following is achieved:

$$\begin{aligned} -(v+1)^2 x_1^4 + 2H_2(v+1) x_1^3 + \left[(v+1)^2\right. \\ \left. - H_3^2 - H_2^2\right] x_1^2 - 2H_2(v+1) x_1 + H_2^2 = 0 \end{aligned} \tag{10}$$

where $x_1 = a_{22}$.

$$H_2^{2/3} + H_3^{2/3} = (v+1)^{2/3} \tag{11}$$

In (10) has four roots at $H_2^{2/3} + H_3^{2/3} < (v+1)^{2/3}$ and two roots at $H_2^{2/3} + H_3^{2/3} > (v+1)^{2/3}$. Therefore, the total number of equilibrium positions for the case where $a_{32} = 0$ and $a_{33} = 0$, i.e., the number of solutions of Group I, can be either 8 or 4, depending on the relation between dimensionless parameters H_2 and H_3.

For the case where $a_{31} \neq 0, a_{32} \neq 0$ and $a_{33} \neq 0$, is necessary to address (9) at $a_{32} \neq 0$ and $a_{33} \neq 0$. After manipulation can be verified that:

$$H_2 H_3 v x_2^2 + \left[H_2^2 + H_3^2 v - 4v(v+1)\right] x_2 + H_2 H_3 = 0 \tag{12}$$

$$\begin{cases} a_{31}^2 = \frac{(H_3 + H_2 x_2)^2 \left(x_2^2+1\right) - 16 x_2^2 (v+1)^2}{16\left(v x_2^2 - 1\right)^2} \\ a_{33}^2 = \frac{16\left(v^2 x_2^2 + 1\right) - (H_3 + H_2 x_2)^2}{16\left(v x_2^2 - 1\right)^2} \end{cases} \tag{13}$$

where:

$$\begin{aligned} x_2 &= \frac{-\left(H_2^2 + H_3^2 v - 4v(v+1)\right) \pm \sqrt{\Delta}}{2 H_3 H_2 v} \text{ and} \\ \Delta &= \left[\left(H_3 + 2\sqrt{v+1}\right)^2 v - H_2^2\right]\left[\left(H_3 - 2\sqrt{v+1}\right)^2 v - H_2^2\right] \end{aligned} \tag{14}$$

The system (9) solution, together with (13), (14), and (5), corresponds to solutions of Group II and does not exceed 8.

For the case where $a_{31} = 0, a_{32} \neq 0$ and $a_{33} \neq 0$, (4) and (5) result in:

$$\begin{cases} 4\left(B a_{22} a_{32} + C a_{23} a_{33}\right) + h_2 a_{32} + h_3 a_{33} = 0 \\ 0 = 0 \\ 0 = 0 \end{cases} \tag{15}$$

$$\begin{cases} a_{21} = 0 \\ 0 = 0 \\ a_{22} a_{32} + a_{23} a_{33} = 0 \end{cases} \tag{16}$$

Utilizing (15) and (16), a 4th order equation in function of $x_3 = a_{22}$ can be obtained:

$$\begin{aligned} -16(v+1)^2 x_3^4 + 8H_2(v+1) x_3^3 + \left(-H_2^2 - H_3^2 + \right. \\ \left. + 16(v+1)^2\right) x_3^2 - 8H_2(v+1) x_3 + H_2^2 = 0 \end{aligned} \tag{17}$$

Like (10), (17) can have either 4 or 2 real roots. Changes in the number of roots on the surface are determined, using the same method as in the Case I, by:

$$H_2^{2/3} + H_3^{2/3} = [4(v+1)]^{2/3} \tag{18}$$

Four roots exist at $H_2^{2/3} + H_3^{2/3} < [4(v+1)]^{2/3}$ and two roots at $H_2^{2/3} + H_3^{2/3} > [4(v+1)]^{2/3}$. Thus, the number of solutions of group III can be either 4 or 8.

Analyzing Fig. 2, the curves (11) and (18) divide the plane (H_3, H_2) in three sub-regions. If $H_2^{2/3} + H_3^{2/3} < [4(v+1)]^{2/3}$, 16 solutions exist (*i.e.* equilibrium positions), 8 solutions for each solutions group I and III; if $(v+1)^{2/3} < H_2^{2/3} + H_3^{2/3} < [4(v+1)]^{2/3}$, there are 12 solutions, 8 from solutions group III and 4 from group I; and if $H_2^{2/3} + H_3^{2/3} > [4(v+1)]^{2/3}$, there are 8 solutions, 4 from each group of solutions I and III. This result is like the ones found by Sarychev et al. (2008).

As mentioned by Sarychev et al. (2005), (13) and (14) need a closer look since they can be valid either for both signs before the square root or for only one sign, which results in the existence of equilibrium positions corresponding to both roots of (12) or only one root ($x_{2,1}$ or $x_{2,2}$). The analysis of the regions of validity of Eqs. (13) and (14) for each root of (12) at $v = 1.5$, considering that $v > 0$, are presented in Fig. 3 and 4. The dashed lines correspond to

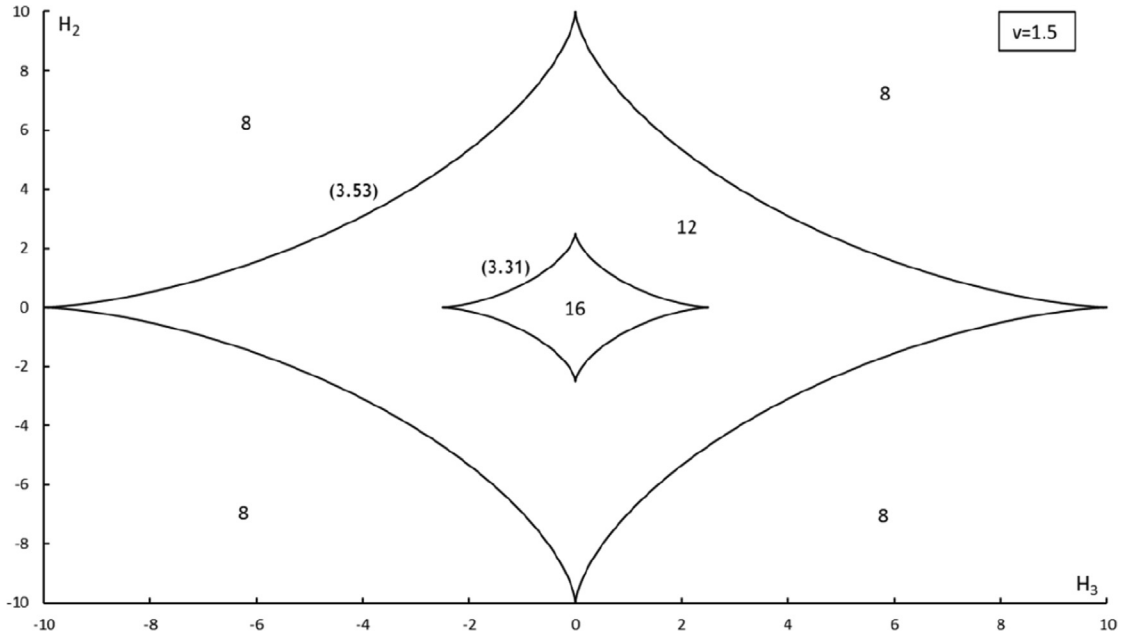

Fig. 2. Bifurcation curves for solutions group I and III for $v = 1.5$.

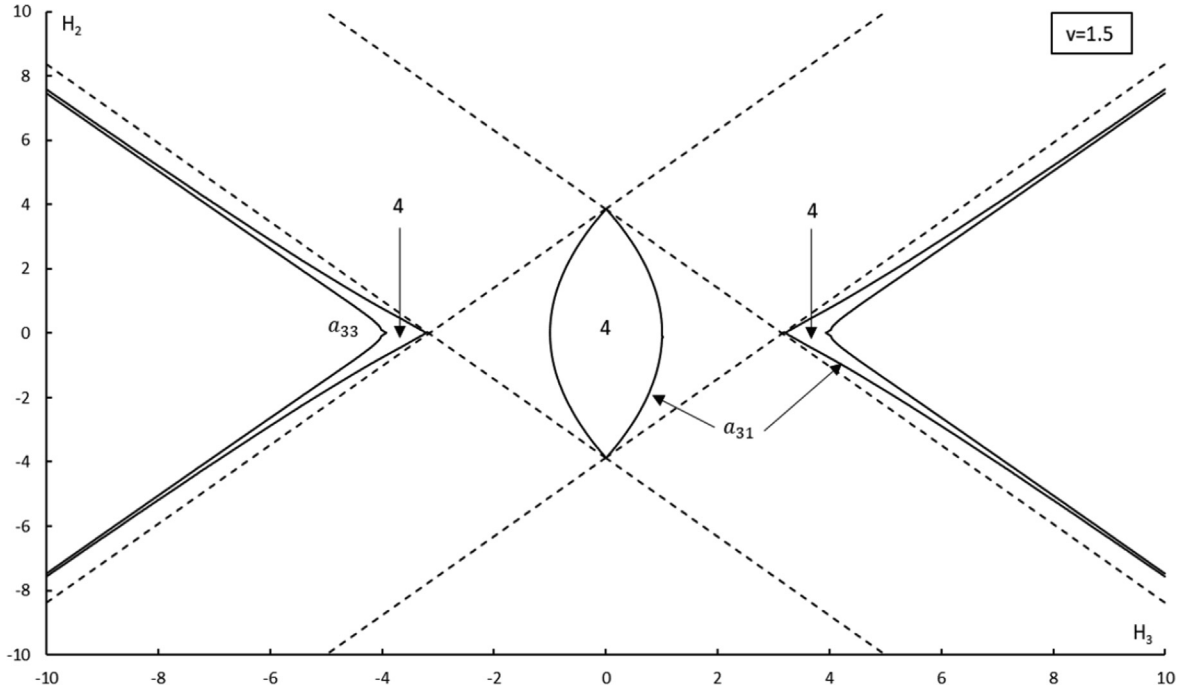

Fig. 3. Regions of validity of the conditions $a_{31}^2 \geqslant 0$ and $a_{33}^2 \geqslant 0$ for the positive root of (13) and (14). at $v = 1.5$.

values where the discriminant (Δ) (14) is equal to zero, which is reflected in more detail in Fig. 5.

For each case presented in Fig. 3 and 4, the full lines represent where expressions (13) and (14) are equal to zero. The areas delimited by full lines are regions where the conditions (13) and (14) are valid for each root of (12). In each of these regions, there are four solutions of Group II; beyond their boundaries, there are no solutions, since one or both conditions (13) and (14) are invalid. Combining the results of Fig. 3 and 4, the study of equilibria bifurcation of Group II is achieved in Fig. 6. The complete equilibria bifurcation study of the gyrostat at $v = 1.5$, combining the study of bifurcation of solutions of Group I, II and III, is presented in Fig. 7. Notice that the plane (H_3, H_2) is portioned into sub-regions. In each sub-region, there are a certain fixed number of equilibrium positions, and the curves are symmetric about the origin of the coordinated axes, as mentioned by Santos (2015).

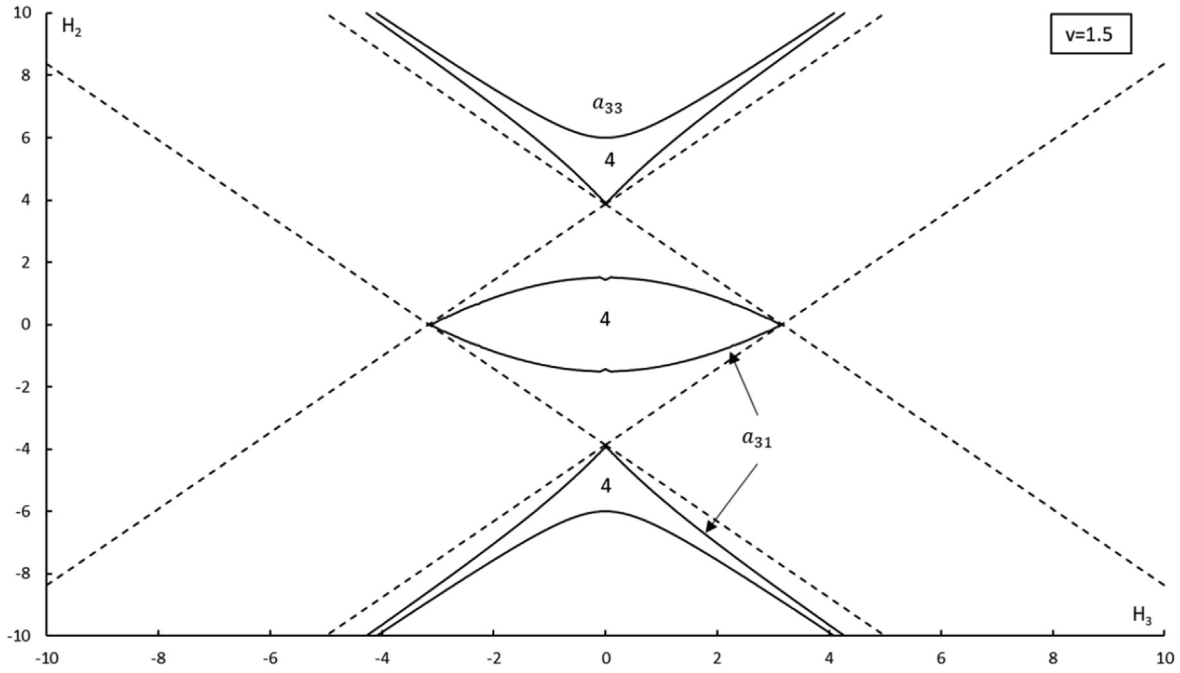

Fig. 4. Regions of validity of the conditions $a_{31}^2 \geqslant 0$ and $a_{33}^2 \geqslant 0$ for the negative root of (13) and (14). at $v = 1.5$.

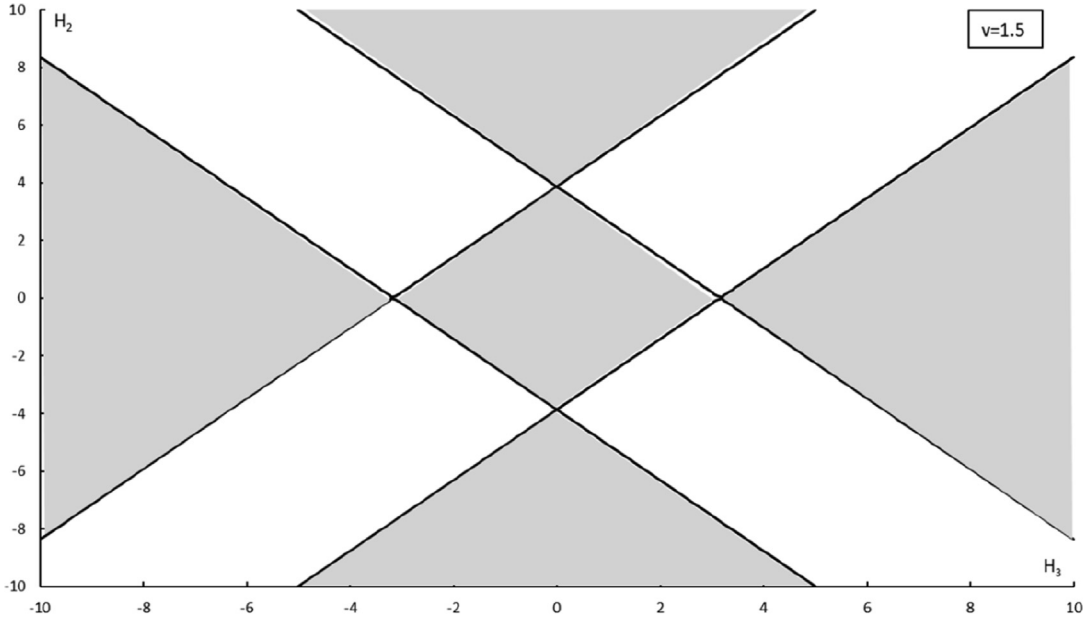

Fig. 5. The regions of validity (gray) of conditions (13) and (14), where $\Delta \geqslant 0$, .for $v = 1.5$.

To help visualise the different conditions of each group I, II and III, presented in Fig. 7, a colour notation is used in Table 1.

One can see from Fig. 7 that there are no more than 24 equilibrium positions and no less than 8 equilibrium positions, the same conclusions were obtained by Saryshev and Mirer (2001), Sarychev et al. (2008), Santos (2015) for other configurations of the gyrostatic moment vector. It is important to mention the two regions of 12 equilibrium positions: (a) and (b). These regions are completely new to the study of this type of gyrostats, they head towards infinity by an oblique asymptote inside a region of eight equilibrium positions. The regions' boundaries distance decreases as they approach infinity and seem to share a relation of parallelism between them.

The evolution of the gyrostat's equilibrium positions along the plane (H_3, H_2), described by the space- craft angles α, β and γ at a specific v, is relevant to show the relation between the gyrostat's equilibria bifurcation curves, shown in Fig. 7, and the behaviour of the spacecraft angles

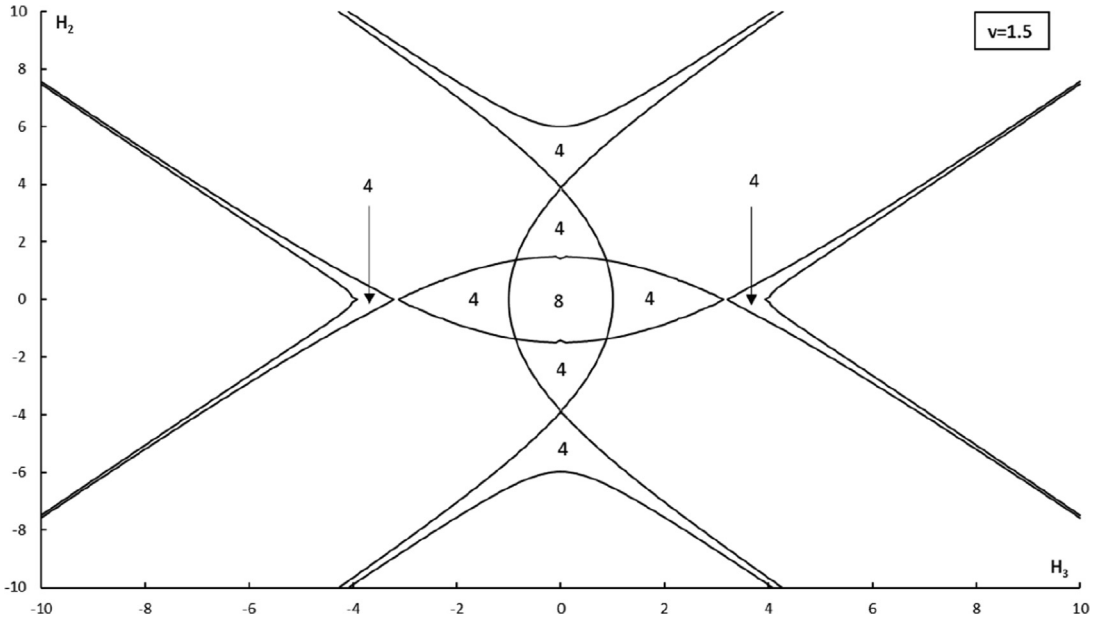

Fig. 6. Bifurcation curves for solutions of Group II at $v = 1.5$.

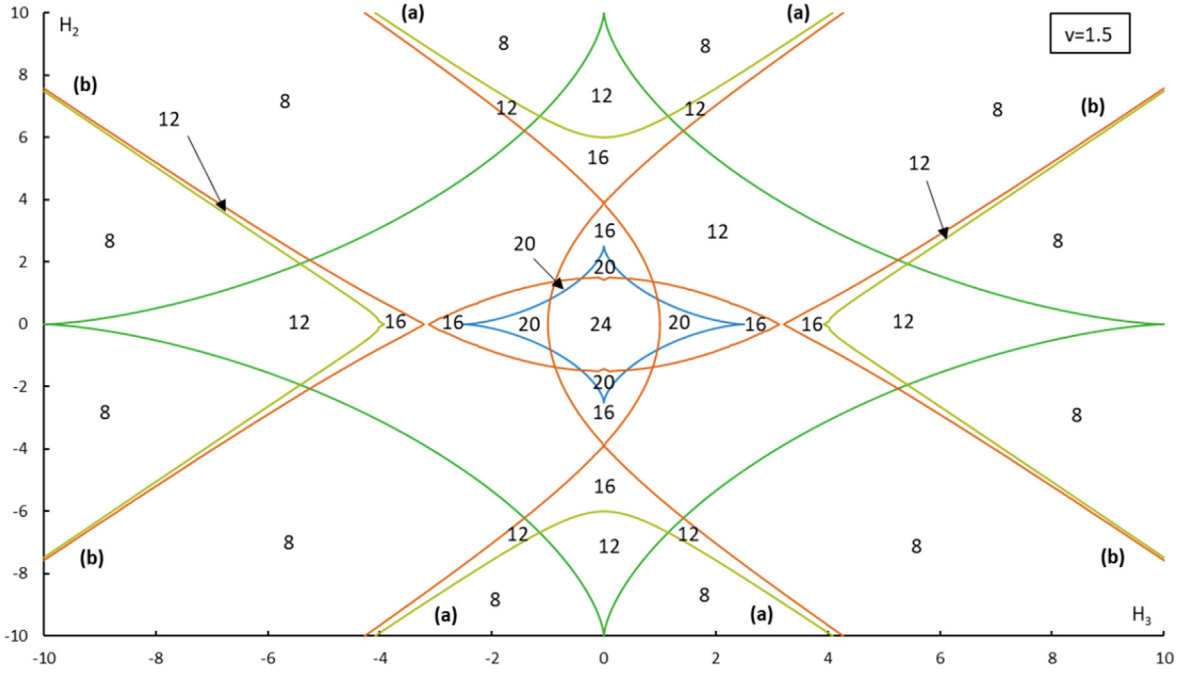

Fig. 7. Gyrostat's equilibria bifurcation at $v = 1.5$.

Table 1
Colour notation of Fig. 7

Curve (Eq. 11)	Curve a^2_{31} (Eq. 13)	Curve a^2_{33} (Eq. 14)	Curve (Eq. 18)
Blue	Orange	Yellow	Green

from these equilibrium solutions. When analysing the coefficients from Eq. (11, 13, 14, 18), the coefficients with odd x degree p_{2k} depend only on odd degree parameters H_2 and H_3. For the coefcients with even x degree p_{2k+1} we can transfer them using a factorized function in a form of $p_{2k+1} = H_2 H_3 a_{2k+1}$, where factor a_{2k+1} depends only on odd degree parameters H_2 and H_3. So, when the sign from H_2 or H_3 is changed, it only changes the sign of real root of

the polynomial (11, 13, 14, 18) while the number of real roots remains unchanged. As so, changing the sign of the real roots has no impact on the number of equilibria regions, and because so, all figures are perfectly symmetrical in both H_2 and H_3 axis. In Fig. 8, the plane's (H_3, H_2) 1st quadrant is shown along with a straight line R (H_3, H_2), at fixed $v = 1.5$, for comparison with Sarychev et al. (2008) and because it goes through each type of region (24, 20, 16, 12 and 8).

Each equilibrium position of groups I and III are determined by choosing one of the roots of (10) and (17), selecting the sign of direction cosine a_{31} (a_{11}) and using the expressions from groups I and III solutions. The roots can have either 4 or 2 real roots depending on whether the ordered pair (H_3, H_2) is before or after the curve (11) and (18). The equilibrium positions for group II are calculated in a more complex way: (a) choose one of the roots of (12); (b) check the validity of conditions: $a_{31}^2 \geqslant 0$ and $a_{33}^2 \geqslant 0$; (c) select the signs of direction cosines a_{31} and a_{33}; and in last, (d) use group II expressions to calculate the other direction cosines. The spacecraft angles α, β and γ are determined using expressions (1).

Following this logic, in Fig. 9, a chart describing the evolution of the spacecraft angles is built corresponding to R (H_3, H_2), and the equilibrium positions index were introduced (see Table 1). The notation used for the equilibrium indexes is adapted from Sarychev et al. (2008), for the sake of comparison. The lines have three different colours: blue, orange, and yellow; and three chart markers: circle, square, and triangle, corresponding to the solutions of group I, II, and III, respectively. The horizontal dashed lines represent: $H_2 = \pi/4, H_2 = \pi/2, H_2 = \pi, H_2 = 3\pi/2$, and $H_2 = 2\pi$, when relevant in the chart.

From the analysis of Fig. 9, there are four values $(R_1 = 0.88, R_2 = 0.94, R_3 = 1.24$ and $R_4 = 3.53)$ at which the fixed number of equilibrium positions changes. For $H_3 \in [0; 0.88]$, there are 24 solutions represented by the indexes (1. (1–8); 2. (1–8) and 3. (1–8)), see Fig. 9 for angle α; at the intersection of straight line $R_1 = 0.88$ and curve (11), four solutions of group I (1. (5–8)) disappear when the angle γ corresponding to these solutions is $\pi/4$.

For $H_3 \in [0.88; 0.94]$, there are 20 solutions (1. (1–4); 2. (1–8) and 3. (1–8)); at the intersection between straight line $R_2 = 0.94$ and curve a_{31} (13), four solutions of group II disappear when the angle β corresponding to these solutions are 0 (2. (6,7)) or 2π (2. (5,8)).

For $H_3 \in [0.94; 1.24]$, there are 16 solutions (1. (1–4); 2. (1–4) and 3. (1–8)); at the intersection between $R_3 = 1.24$ and curve a_{31} (13), the last four solutions of group II disappear when the angle β corresponding to these solutions is 0 (2. (1,4)) or 2π (2. (2,3)).

For $H_3 \in [1.24; 3.53]$, there are 12 solutions (1. (1–4) and 3. (1–8)); at the intersection between R4 $= 3.53$ and curve (18), four solutions of group III (3. (5–8)) disappear when the angle γ corresponding to these solutions is $\pi/4$. At $R > 3.53$ until the end of the window of Fig. 8, there are only 8 solutions (1. (1–4) and 3. (1–4)), the values of angles α and β remain constant and the angle γ tends to a constant value as R increases, for each solution.

Fig. 10 shows the bifurcation of equilibria for $v = 0.7$. The results show that for every inertial configuration studied, there are no less than 8 equilibrium positions and no more than 24. In a general way, in regions with small values of H_3 and H_2, there are 24 equilibrium positions. With the increase of H_3 and/or H_2, the 24 equilibrium positions region gives place to 20 equilibrium positions region, then

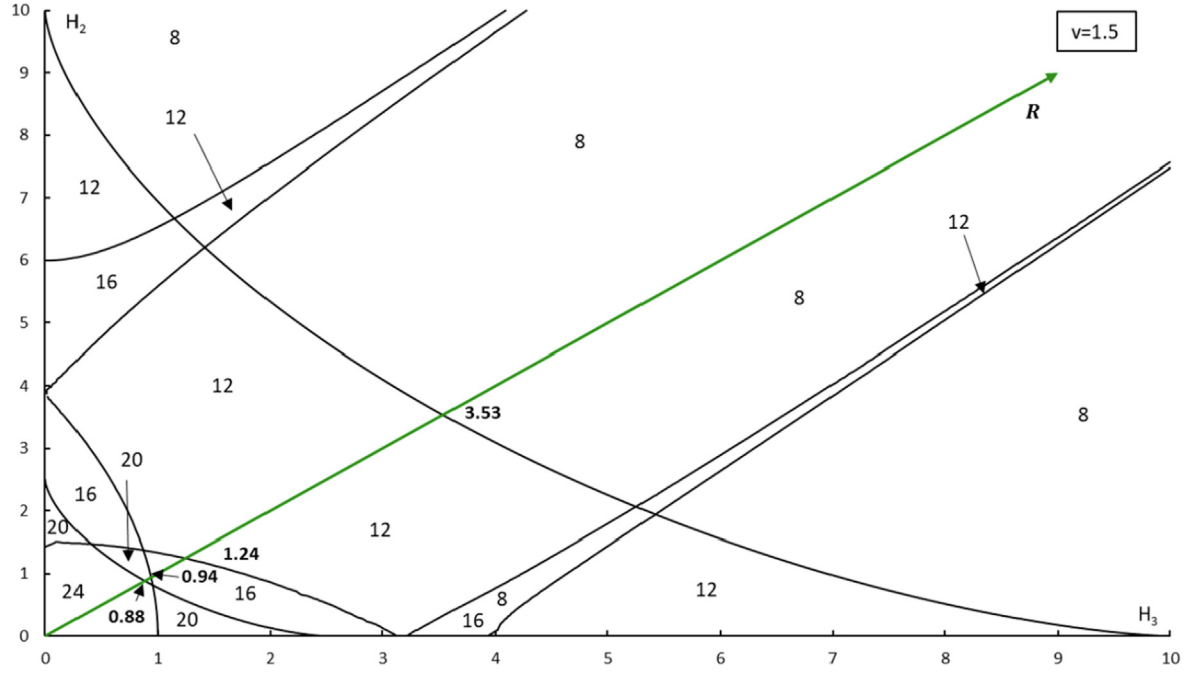

Fig. 8. Gyrostat's equilibria bifurcation at $v = 1.5$ and straight line R (H_3, H_2) with bifurcation values.

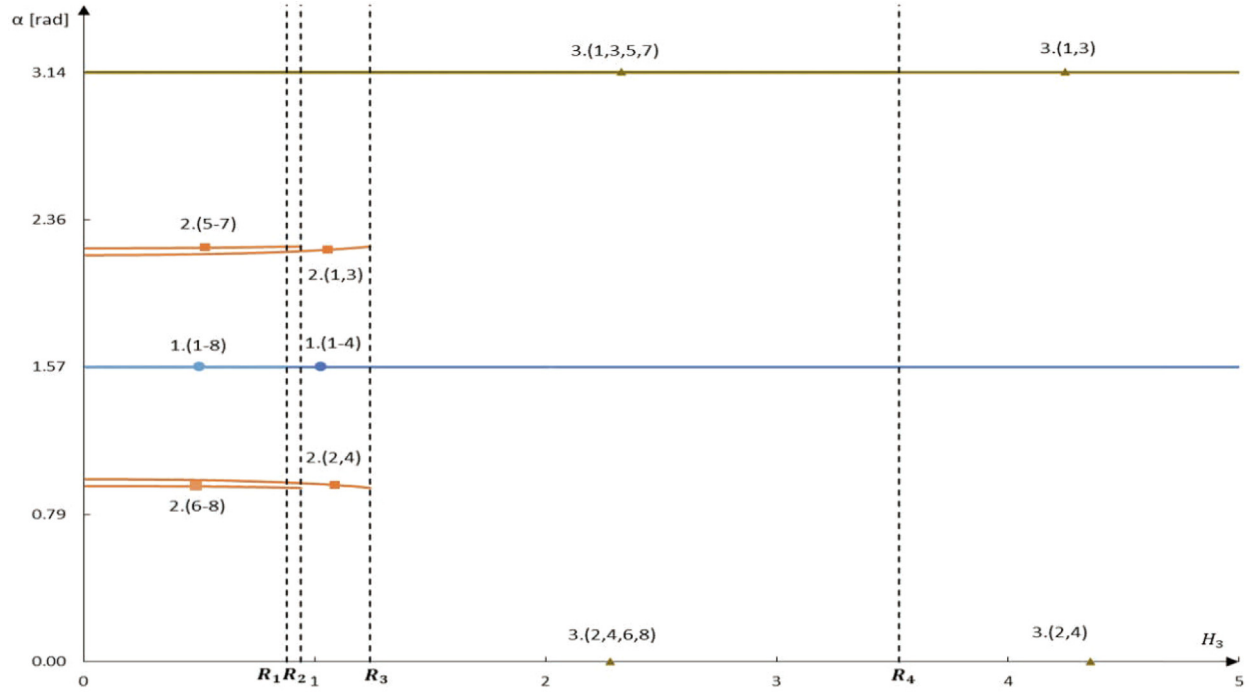

(a) Equilibrium positions described by α

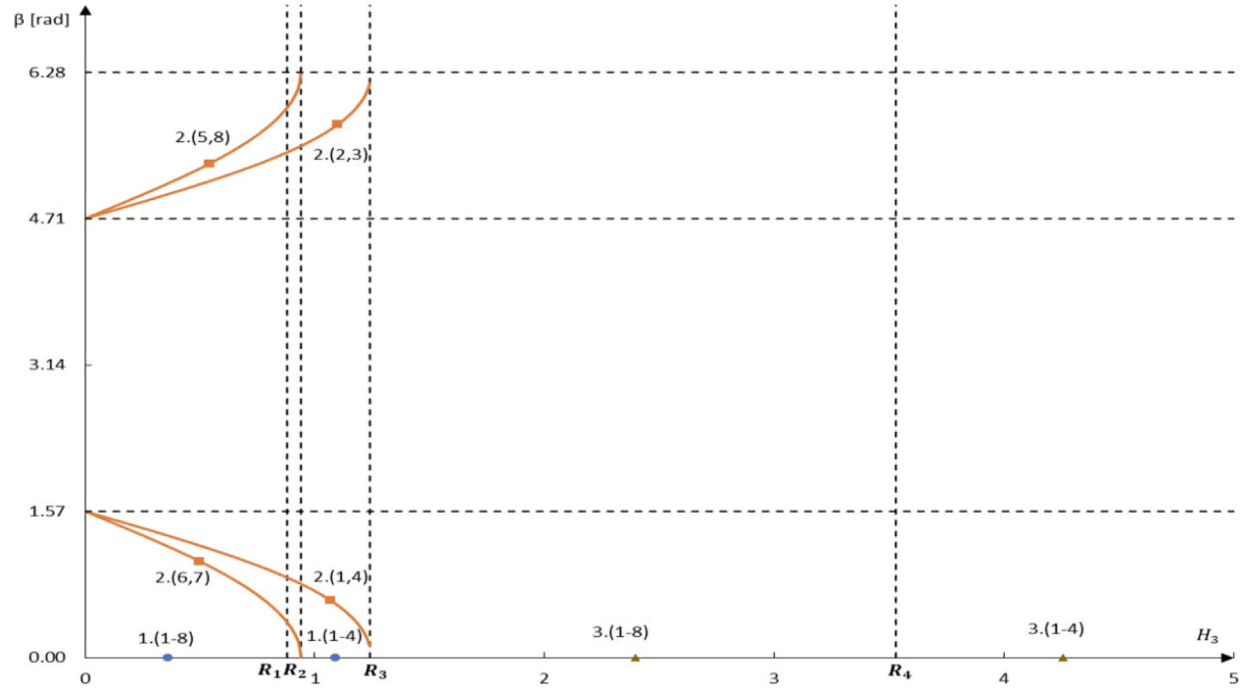

(b) Equilibrium positions described by β

Fig. 9. Equilibrium positions of a gyrostat at $v = 1.5$ and for R $(H_2 = H_3)$ described by angles α, β and γ.

to 16 equilibrium positions region, then to 12 equilibrium positions region and finally, to 8 equilibrium positions region. There can be also found some peculiarities in this study: two small regions of 12 equilibrium positions, which tend to infinity, and two regions of 16 equilibrium positions inside one of 12 equilibria positions that exist outside the main regions. The upper region of 16 equilibrium positions and 12 equilibria positions approaches an oblique asymptote, which slope is low for lower values of $v(v = 0.1)$, but increases as v increases. The regions' boundaries distance also increases with the value of v. On the other hand, the lower region of 16 equilibria positions and 12 equilibria positions also approaches an oblique asymptote, almost in a parallel way with the previous case, which slope is low for

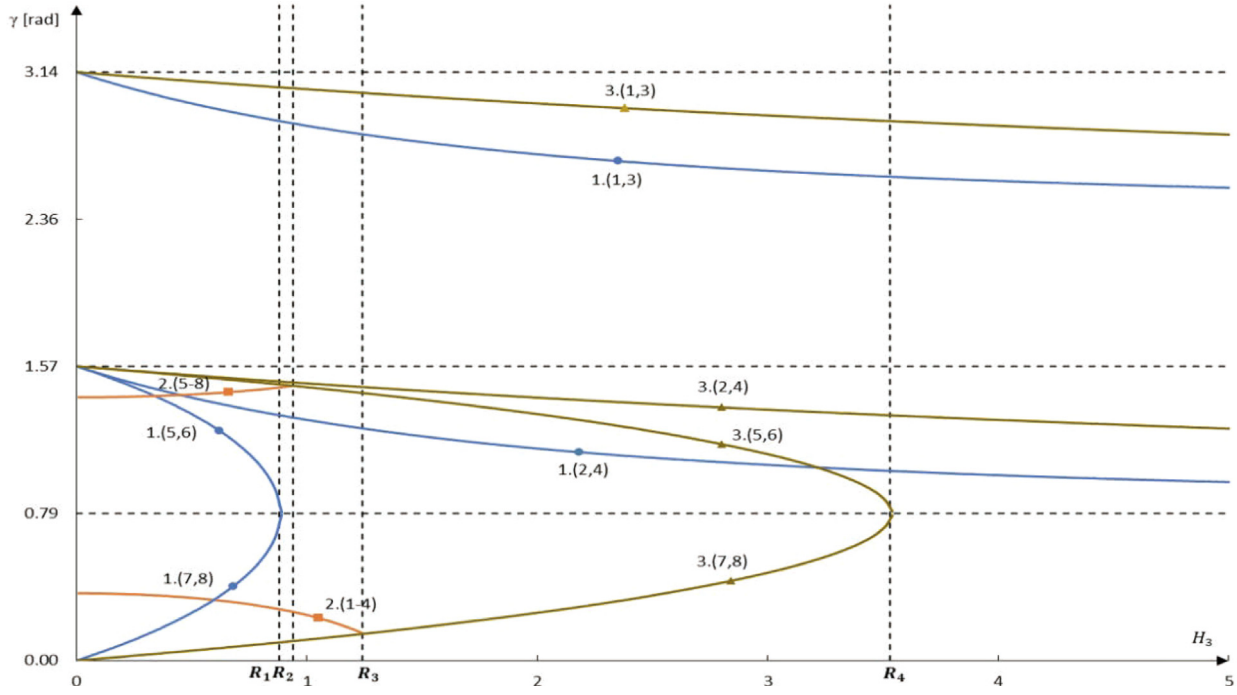

(c) Equilibrium positions described by γ

Fig 9. *(continued)*

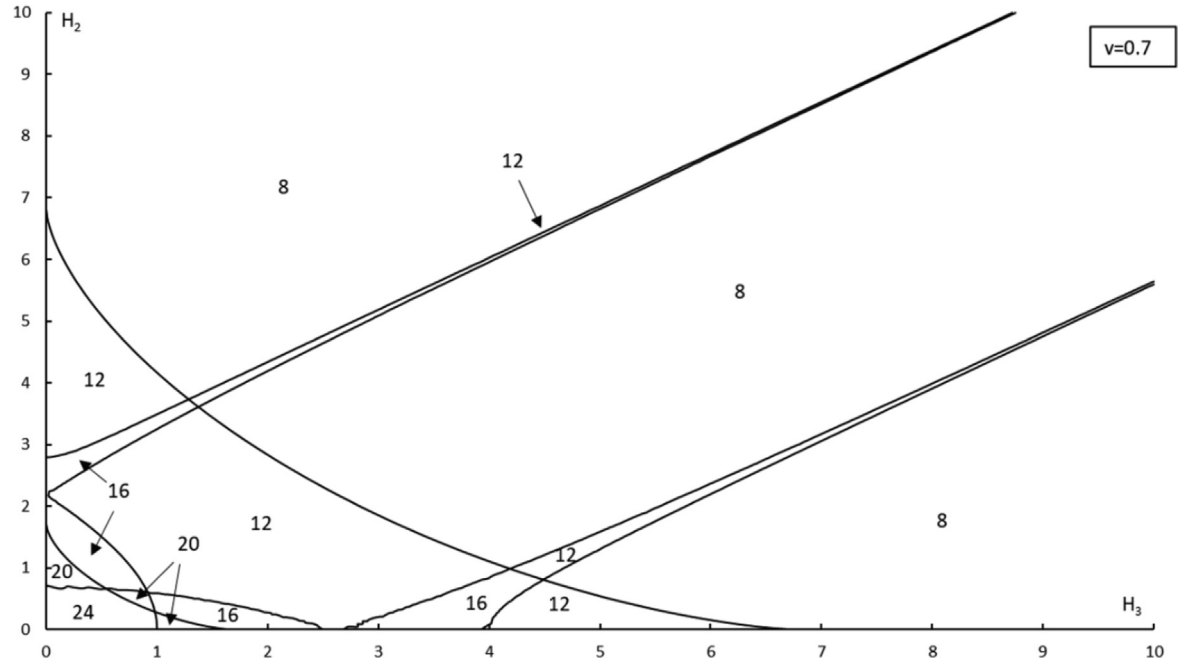

Fig. 10. Gyrostat's equilibria bifurcation at $v = 0.7$.

lower values of v and high for higher values of v. However, the regions' boundaries distance differs from the previous case, as it diminishes with higher values of v. A different case happens with a small region of 16 equilibria positions inside one of 20 equilibria positions, like the ones found by Sarychev et al. (2008), derived from a_{31}^2 expression, which exist near $H_3 = 0$ and $H_2 = 0.5$ for $v < 0.3$ and near $H_3 = 4$ and $H_2 = 0$ for $v \geqslant 4$. These regions increase in size with lower values of $v(v < 0.3)$ and higher values of $v(v \geqslant 4)$.

4. Gyrostat's Stability of Equilibria

In this section, Lyapunov's stability theory is reviewed and the sufficient stability conditions for the equilibrium positions of a gyrostat satellite are obtained. As in previous studies (Sarychev et al., 2008; Santos, 2015), the generalized energy integral is continuous, and it can therefore be used as Lyapunov's function:

$$\begin{aligned}&\tfrac{1}{2}\left(A\overline{p}^2+Bq^2+C\overline{r}^2\right)+\\&+\tfrac{1}{2}\omega_0^2\left[3\left[(A-C)\,a_{31}^2+(B-C)\,a_{32}^2\right]+\right.\\&+\left[(B-A)\,a_{21}^2+(B-C)\,a_{23}^2\right]\\&\left.-2(C-A)(H_2a_{22}+H_3a_{23})\right]=H\end{aligned}\tag{19}$$

Now, small variations will be introduced in the direction angles. These variations can be interpreted as orbital disturbances since the main purpose is to check how the system will respond to disturbances near α,β and γ. Thus, let us represent α,β and γ in the form:

$$\begin{cases}\alpha=\alpha_0+\overline{\alpha}\\ \beta=\beta_0+\overline{\beta}\\ \gamma=\gamma_0+\overline{\gamma}\end{cases}\tag{20}$$

Where α,β and γ are small deviations from the satellite's equilibrium position: $\alpha=\alpha_0=const,\beta=\beta_0=const$ and $\gamma=\gamma_0=const$. Then, the energy integral can be written in the following form:

$$\begin{aligned}&\tfrac{1}{2}\left(A\overline{p}^2+Bq^2+C\overline{r}^2\right)+\\&+\tfrac{1}{2}\omega_0^2\left(A_{\alpha\alpha}\overline{\alpha}^2+A_{\beta\beta}\overline{\beta}^2+A_{\gamma\gamma}\overline{\gamma}^2+\right.\\&\left.+2A_{\alpha\beta}\overline{\alpha}\overline{\beta}+2A_{\beta\gamma}\overline{\beta}\overline{\gamma}+2A_{\alpha\gamma}\overline{\alpha}\overline{\gamma}\right)+\sum=const\end{aligned}\tag{21}$$

Where Σ designates the terms of higher than second order of smallness with respect to $\overline{\alpha},\overline{\beta},\overline{\gamma}$. Expanding the direction cosines according to a Taylor series (Santos and Melicio, 2020):

$$\begin{aligned}&a_{ij}(\alpha,\beta,\gamma)=a_{ij}\left(\alpha_0+\overline{\alpha},\beta_0+\overline{\beta},\gamma_0+\overline{\gamma}\right)=\\&=a_{ij}(\alpha_0,\beta_0,\gamma_0)+\left(\tfrac{\partial\overline{a_{ij}}}{\partial\alpha}\overline{\alpha}+\tfrac{\partial\overline{a_{ij}}}{\partial\beta}\overline{\beta}+\tfrac{\partial\overline{a_{ij}}}{\partial\gamma}\overline{\gamma}\right)+\\&+\tfrac{1}{2}\left(\tfrac{\partial^2\overline{a_{ij}}}{\partial\alpha^2}\overline{\alpha}^2+\tfrac{\partial^2\overline{a_{ij}}}{\partial\beta^2}\overline{\beta}^2+\tfrac{\partial^2\overline{a_{ij}}}{\partial\gamma^2}\overline{\gamma}^2+\right.\\&\left.+2\tfrac{\partial^2\overline{a_{ij}}}{\partial\alpha\partial\beta}\overline{\alpha}\overline{\beta}+2\tfrac{\partial^2\overline{a_{ij}}}{\partial\alpha\partial\gamma}\overline{\alpha}\overline{\gamma}+2\tfrac{\partial^2\overline{a_{ij}}}{\partial\beta\partial\gamma}\overline{\beta}\overline{\gamma}\right)\end{aligned}\tag{22}$$

To study the stability of small displacements, the expanded Taylor series above must be applied to the system of direction cosines (1). Afterwards, when applied the small displacements described in (20), the system (1) is transformed into:

$$\begin{cases}\overline{a_{11}}=\cos\alpha_0\cos\beta_0\\ \overline{a_{12}}=\cos\alpha_0\sin\gamma_0-\cos\alpha_0\sin\beta_0\sin\gamma_0\\ \overline{a_{13}}=\cos\alpha_0\cos\gamma_0+\cos\alpha_0\sin\beta_0\sin\gamma_0\\ \overline{a_{21}}=\sin\beta_0\\ \overline{a_{22}}=\cos\beta_0\cos\gamma_0\\ \overline{a_{23}}=-\cos\beta_0\sin\gamma_0\\ \overline{a_{31}}=-\sin\alpha_0\cos\beta_0\\ \overline{a_{32}}=\cos\alpha_0\sin\gamma_0+\sin\alpha_0\sin\beta_0\cos\gamma_0\\ \overline{a_{33}}=\cos\alpha_0\cos\gamma_0-\sin\alpha_0\sin\beta_0\sin\gamma_0\end{cases}\tag{23}$$

After applying the Taylor series described in (22) to the system of direction cosines only for the relevant direction cosines $a_{21},a_{22},a_{23},a_{31}$, and a_{32}, the following expressions are obtained:

$$\begin{cases}A_{\alpha\alpha}=[3(A-C)(\overline{a_{11}}^2-\overline{a_{31}}^2)+(B-C)(\overline{a_{12}}^2-\overline{a_{32}}^2)]\\ A_{\beta\beta}=(B-C)\left[3\left(\overline{a_{22}}^2\sin^2\alpha_0-\overline{a_{32}}\,\overline{a_{21}}\cos\gamma_0\sin\alpha_0\right)+\right.\\ \quad\left.+\overline{a_{21}}^2\sin^2\gamma_0-\overline{a_{23}}^2\right]+(B-A)(\cos^2\beta_0-\overline{a_{21}}^2)+\\ \quad+(A-C)\left[3\left(\overline{a_{21}}^2\sin^2\alpha_0-\overline{a_{31}}^2\right)-H_2\overline{a_{22}}-H_3\overline{a_{23}}\right]\\ A_{\gamma\gamma}=(B-C)[(\overline{a_{22}}^2-\overline{a_{23}}^2)-3(\overline{a_{32}}^2-\overline{a_{33}}^2)]\\ \quad-(A-C)(H_2\overline{a_{22}}+H_3\overline{a_{23}})\\ A_{\alpha\beta}=3(A-C)(\overline{a_{21}}\,\overline{a_{31}}\cos\alpha_0-\overline{a_{11}}\,\overline{a_{21}}\sin\alpha_0)+\\ \quad+3(B-C)(\overline{a_{11}}\,\overline{a_{32}}\cos\gamma_0-\overline{a_{12}}\,\overline{a_{22}}\sin\alpha_0)\\ A_{\beta\gamma}(B-C)[\overline{a_{21}}(\overline{a_{23}}\cos\gamma_0-\overline{a_{22}}\sin\gamma_0)+\\ \quad+3\sin\alpha_0(\overline{a_{22}}\,\overline{a_{33}}+\overline{a_{23}}\,\overline{a_{32}})]+\\ \quad+(A-C)\,\overline{a_{21}}(H_2\sin\gamma_0+H_3\cos\gamma_0)\\ A_{\alpha\gamma}=-3(B-C)(\overline{a_{12}}\,\overline{a_{33}}+\overline{a_{13}}\,\overline{a_{32}})\end{cases}\tag{24}$$

Sarychev et al. (2008), Santos (2015) is stated that from the Lyapunov's theorem, the equilibrium solution $\alpha=\alpha_0,\beta=\beta_0$ and $\gamma=\gamma_0$ is asymptotically stable if the quadratic form:

$$\begin{aligned}&A_{\alpha\alpha}\overline{\alpha}^2+A_{\beta\beta}\overline{\beta}^2+A_{\gamma\gamma}\overline{\gamma}^2+\\&+2A_{\alpha\beta}\overline{\alpha}\overline{\beta}+2A_{\beta\gamma}\overline{\beta}\overline{\gamma}+2A_{\alpha\gamma}\overline{\alpha}\overline{\gamma}\end{aligned}\tag{25}$$

is positive definite, *i.e.*, at:

$$\begin{cases}A_{\alpha\alpha}>0\\ A_{\alpha\alpha}A_{\beta\beta}-A_{\alpha\beta}>0\\ A_{\alpha\alpha}A_{\beta\beta}A_{\gamma\gamma}+2A_{\alpha\beta}A_{\beta\gamma}A_{\alpha\gamma}\\ \quad-A_{\alpha\alpha}A_{\beta\gamma}^2-A_{\beta\beta}A_{\alpha\gamma}^2-A_{\gamma\gamma}A_{\alpha\beta}^2>0\end{cases}\tag{26}$$

Now it is necessary to test the solutions obtained in Chapter 3, *i.e.*, test the equilibria solutions into the Lyapunov's stability theory's scheme presented in (26).

For Group I solutions the following is presented:

$$A_{\alpha\alpha}>0\Longleftrightarrow 1-(v+1)\frac{H_3^2x_1^2}{(H_2-x_1(v+1))^2}>0\tag{27}$$

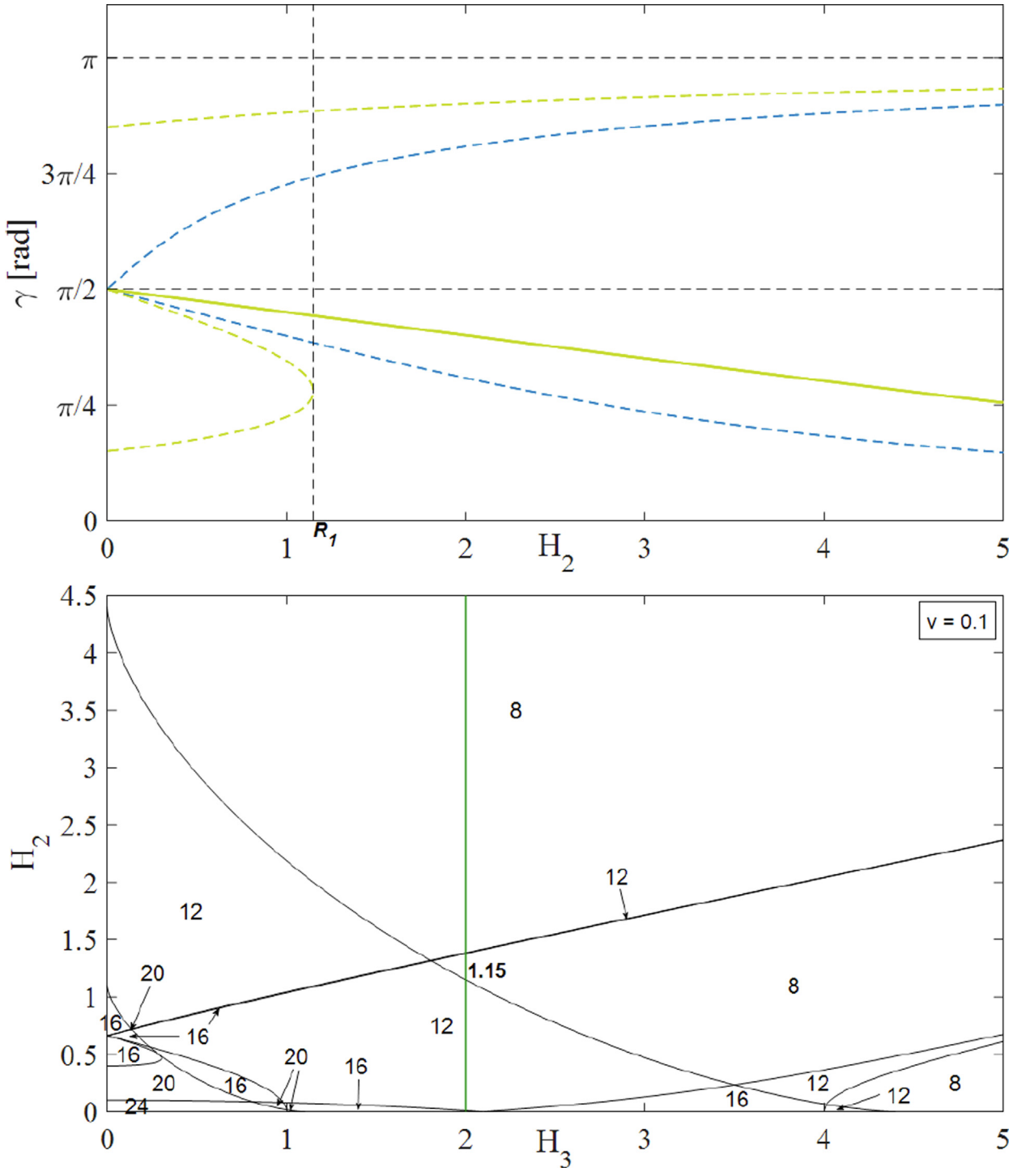

Fig. 11. Stability as a function of angle γ and H_2 (a) and respective equilibria chart for $v = 0.1$ and $H_3 = 2$ (b).

$$
\begin{aligned}
&A_{\alpha\alpha}A_{\beta\beta} - A_{\alpha\beta}^2 > 0 \iff \\
&\iff 3\left[1-(v+1)\frac{H_3^2 x_1^2}{(H_2 - x_1\,(v+1))^2}\right]\times \\
&\left\{-(v+1)\left[3x_1^2\sin^2\alpha_0 - \frac{H_3^2 x_1^2}{(H_2 - x_1\,(v+1))^2}\right]\right. \\
&\left.-v\cos^2\beta_0 + 3 + H_2 x_1 + \frac{H_3^2 x_1}{H_2 - x_1\,(v+1)}\right\} \\
&-9(v+1)^2\frac{H_3^2 x_1^4}{(H_2 - x_1\,(v+1))^2}\sin\alpha_0 > 0
\end{aligned}
\tag{28}
$$

The stability study of the group II solutions leads to a more complex problem. In this case, the relations ((12)–(14)) should be used to determine a_{31}, a_{32}, and a_{33}, and the group II solutions for the rest of the direction cosines matrix elements. Then, the angles α_0, β_0 and γ_0 are determined explicitly and the coefficients of the quadratic form (24) are calculated, as well as the conditions of its positive definiteness. Using this direct approach, this problem was impossible to solve, and the usage of a different method to

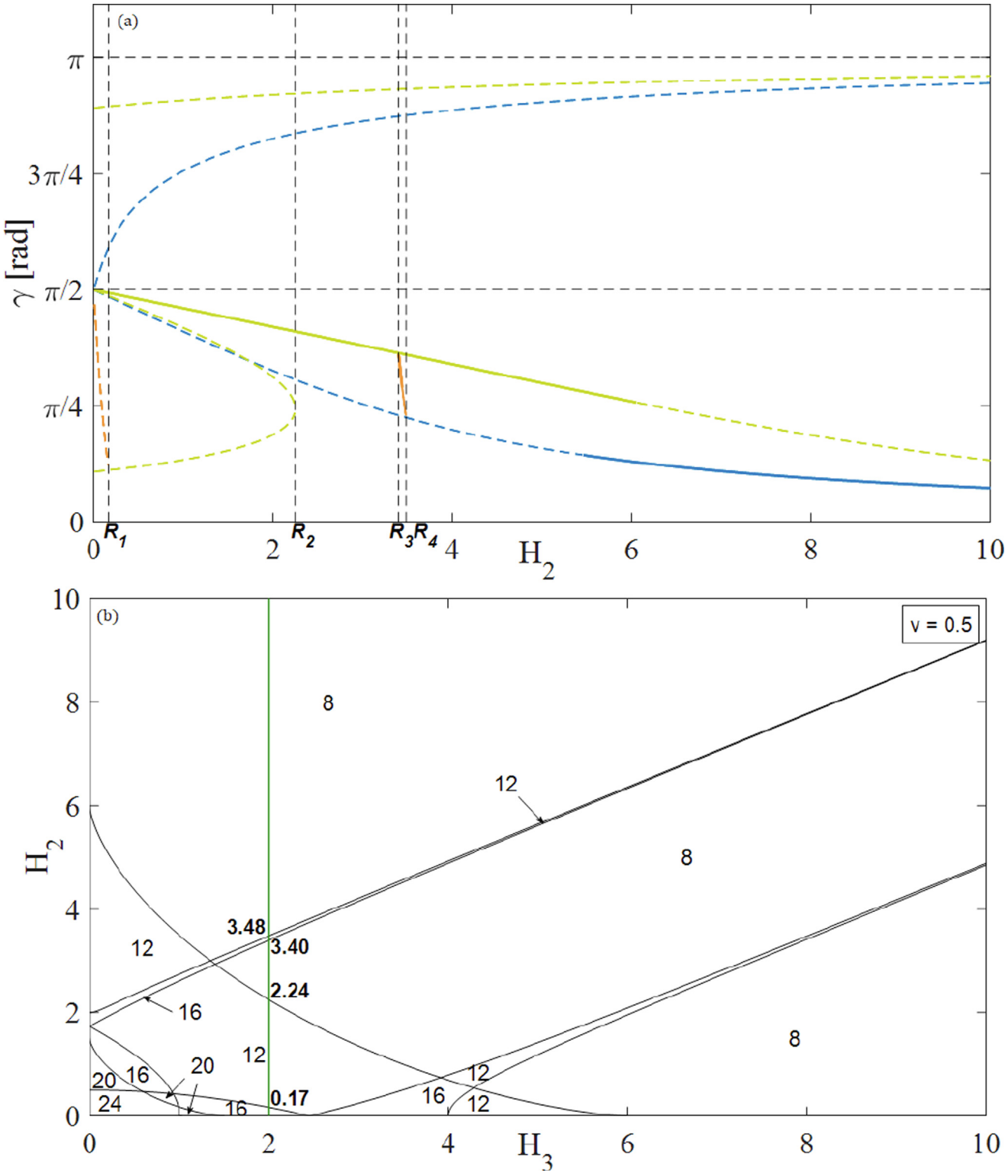

Fig. 12. Stability as a function of angle γ and H_2 (a) and respective equilibria chart for $v = 0.5$ and $H_3 = 2$ (b).

analytically achieve the group II stability of equilibria equations is recommended. Nevertheless, the solutions were computed using mathematical software and results were added to the graphical analysis.

For Group III solutions, the following is presented:

$$A_{\alpha\alpha} > 0 \Longleftrightarrow 1 - (v+1)\frac{H_3^2 x_3^2}{(H_2 - 4(v+1)x_3)^2} > 0 \qquad (29)$$

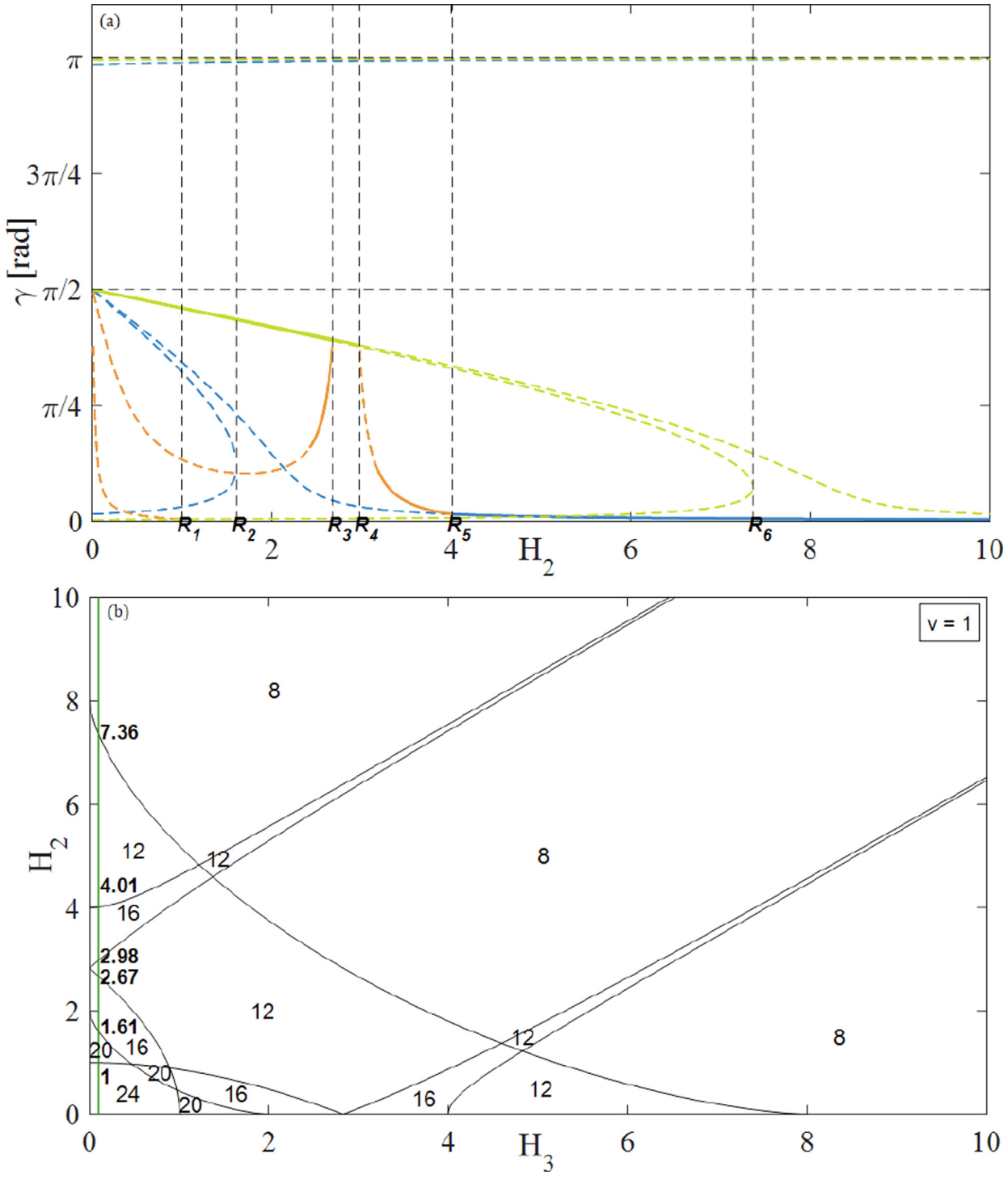

Fig. 13. Stability as a function of angle γ and H_2 (a) and respective equilibria chart for $v = 1.0$ and $H_3 = 0.1$ (b).

$$
\begin{aligned}
&A_{\alpha\alpha}A_{\beta\beta} - A_{\alpha\beta}^2 > 0 \iff \\
&\iff 3\left[-1 + (v+1)\frac{H_3^2 x_3^2}{(H_2 - 4(v+1)x_3)^2}\right] \times \\
&\left\{(v+1)\frac{H_3^2 x_3^2}{(H_2 - 4(v+1)x_3)^2} - v\cos^2\beta_0 + \right. \\
&\left. + H_2 x_3 + \frac{H_3^2 x_3}{H_2 - 4(v+1)x_3}\right\} \\
&-9(v+1)^2\frac{H_3^2 x_3^2}{(H_2 - 4(v+1)x_3)^2}\cos\gamma_0 > 0
\end{aligned}
\tag{30}
$$

The graphical results from the stability analysis are shown in Fig. 11–16 as a function of spacecraft angle γ and H_2. The coloured dashed lines correspond to when a specific equilibrium position is unstable, and the coloured full lines correspond to when a specific equilibrium position is stable (sufficient conditions of stability (24) are valid). The colours blue, orange, and dark yellow represent equilibrium solutions of group I, II, and III, respectively. The black vertical dashed lines (R_i) in the stability chart correspond

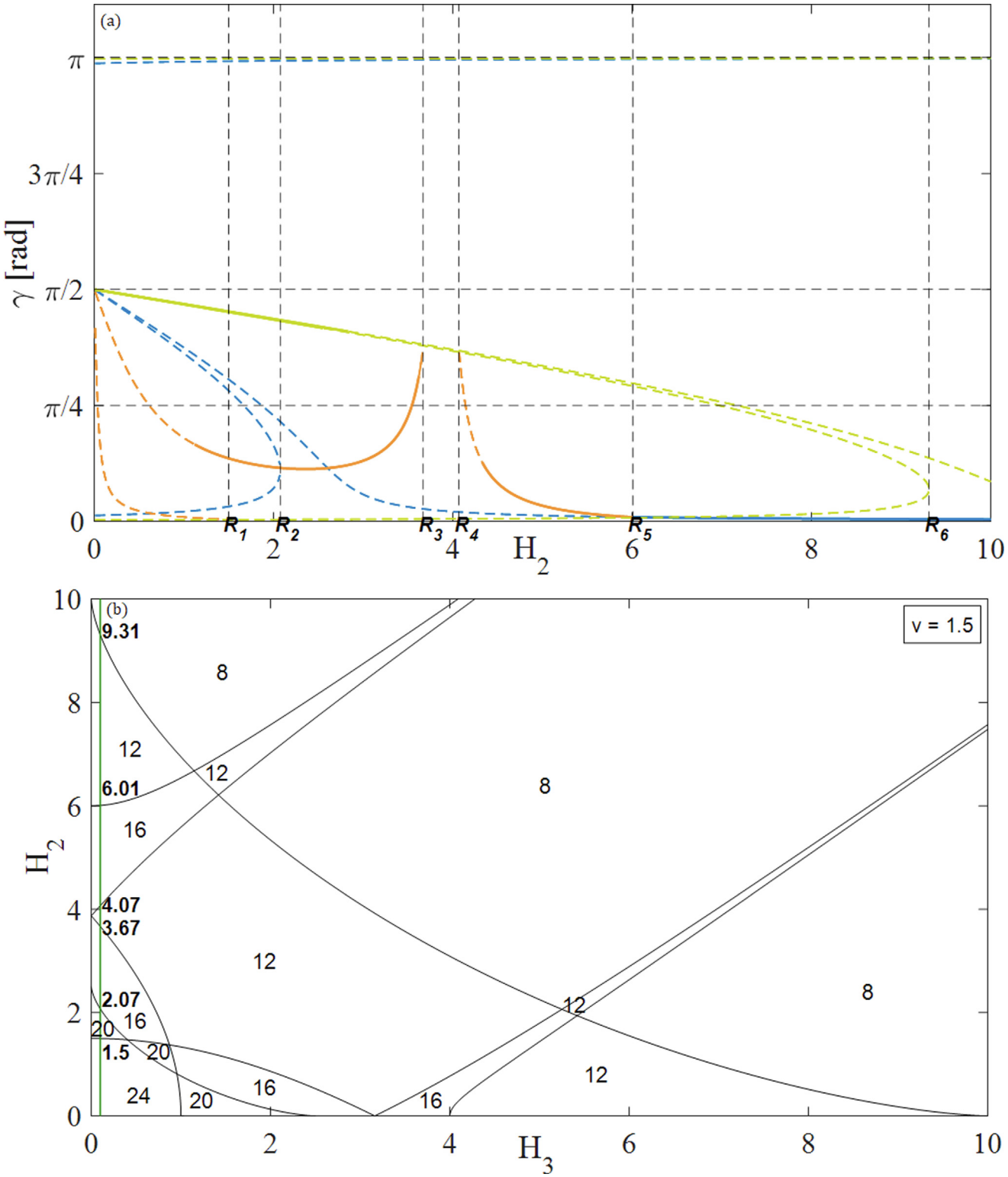

Fig. 14. Stability as a function of angle γ and H_2 (a) and respective equilibria chart for $v = 1.5$ and $H_3 = 0.1$ (b).

to intersection points ($i = 1, 2, \ldots$) between the green line and equilibria regions, in the equilibria chart. Finally, the black horizontal dashed line corresponds to notable points ($\pi/2$ and π) in the axis γ $[rad]$.

The results obtained for all cases, in the first place, show that the angle γ can vary between 0 and π; second, there is a minimum of two stable equilibrium solutions and a maximum of six stable equilibrium positions

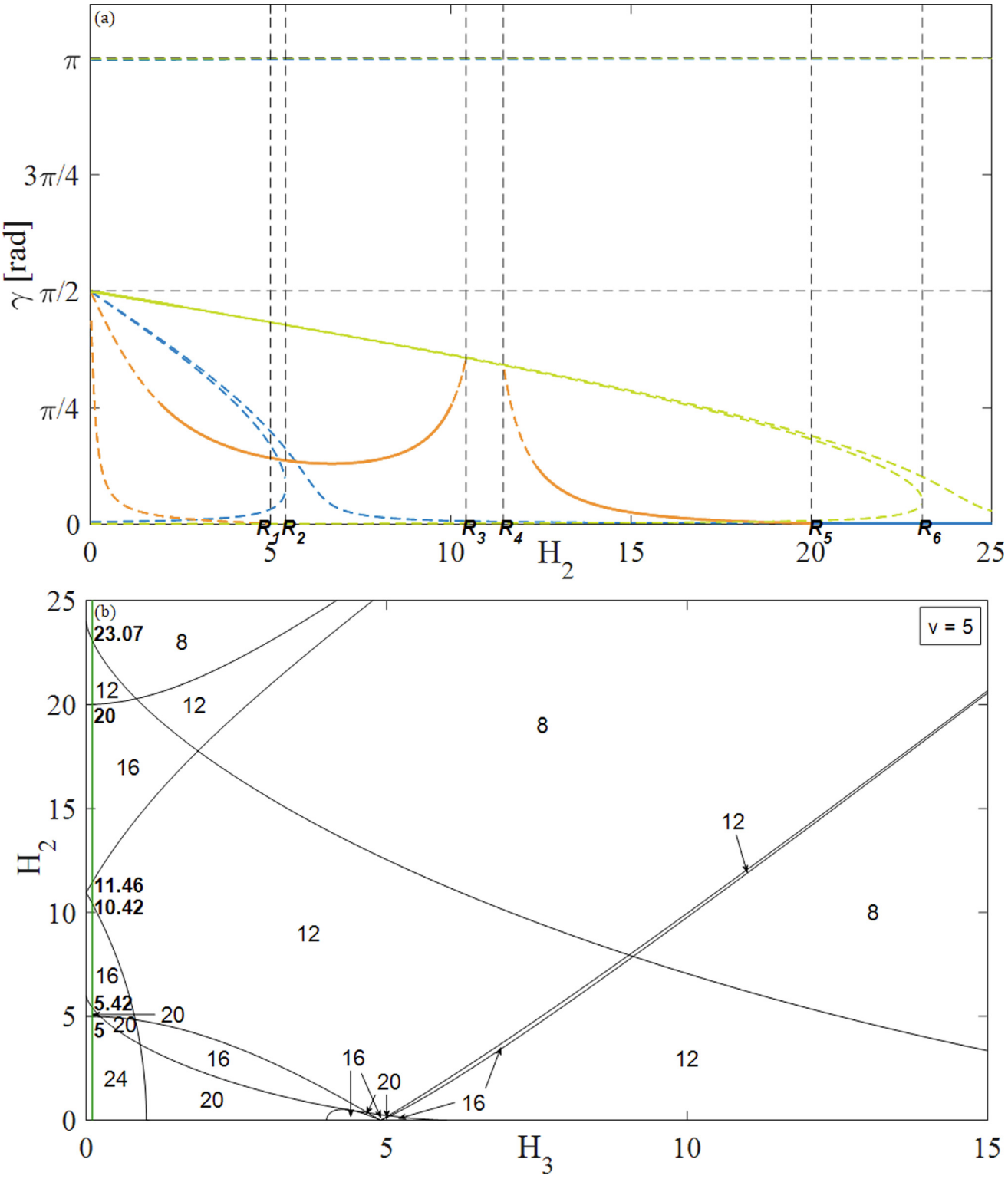

Fig. 15. Stability as a function of angle γ and H_2 (a) and respective equilibria chart for $v = 5$ and $H_3 = 5$ (b).

for each analysed case. For each group of two consecutive equilibrium positions from group I and III, the angle γ value is the same. This means that each equilibrium curve in each chart represents two equilibrium positions.

In the case of group II, it has also been proven that the eight equilibrium positions can be reduced to two equilibrium curves in each chart. Analysing the stability of these solutions, for the same value of angle γ, a group of four solutions can have two stable solutions and two unstable

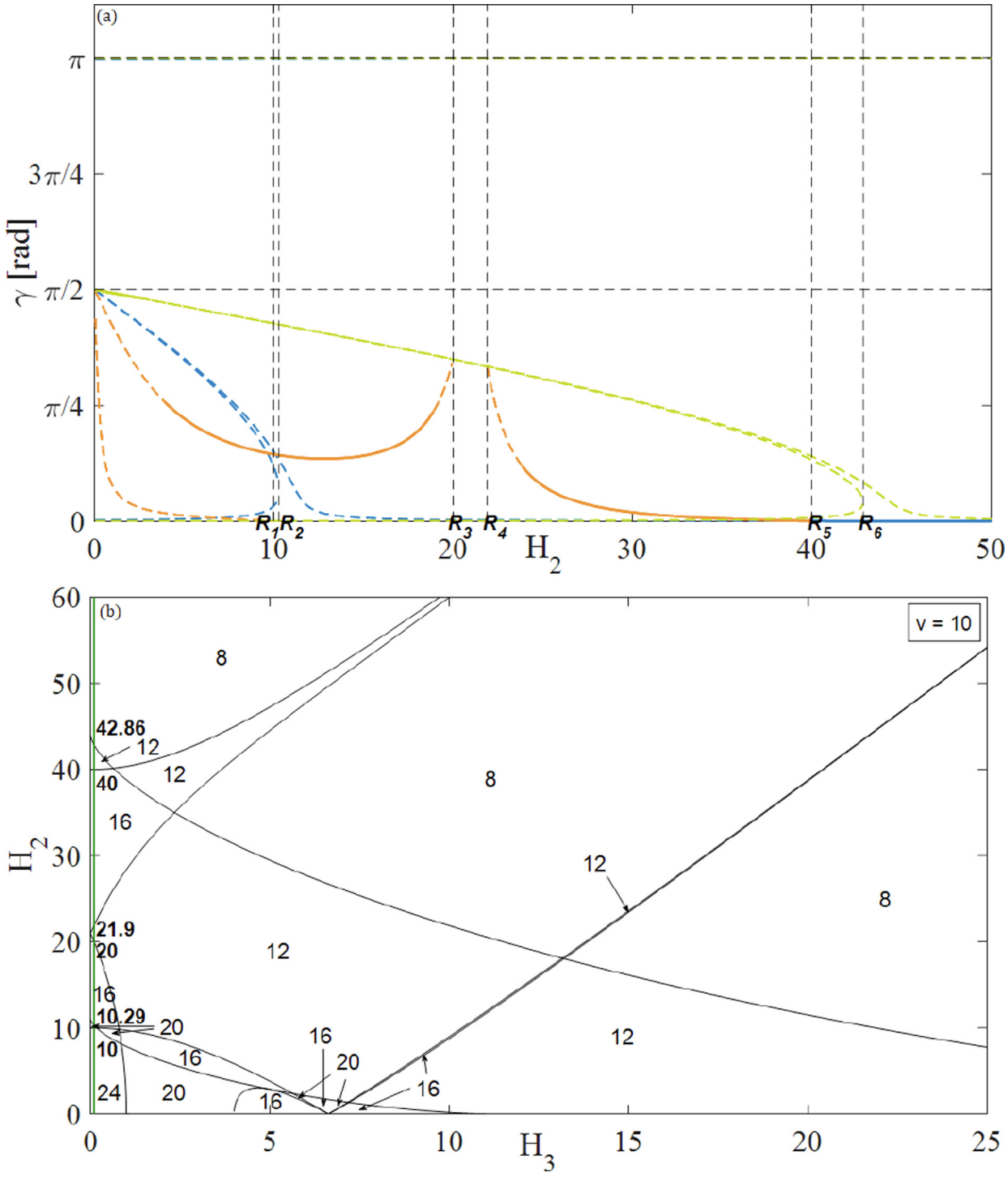

Fig. 16. Stability as a function of angle γ and H_2 (a) and respective equilibria chart for $v = 10$ and $H_3 = 0.1$ (b).

solutions simultaneously. An example can be seen in Fig. 15 between R_4 and R_5, where a full line matches a dashed line. This discovery is entirely new in the gyrostat satellite stability study and should be further analysed in future work.

For lower values of v ($v = 0.1$ and $v = 0.5$), the regions defined by the upper oblique asymptote became very narrow, which also makes the equilibrium curves very narrow or even disappear, Fig. 11 and 12. For higher values of v ($v = 5$ and $v = 10$), similarly, the regions defined by the lower oblique asymptote became very narrow, which makes the equilibrium curves have small intervals or vanish, Fig. 15 and 16. For high values of H_3 ($H_3 \neq 10$), both regions mentioned before became very narrow, which has the same consequence as previous cases.

The increase of parameter H_2, in the case of group I and III, makes the equilibrium curves converge to a certain angle γ. In the case of group II, the parameter increase

can make the equilibrium curves vanish, this happens at intersection points (R_i) that result from the bisection of the vertical line $H_3 = const$ with the regions' borders with a fixed number of equilibria.

Finally, analysing the case when v varies and H_3 is constant (*e.g.*, $H_3 = 0.1$, Fig. 13, 14, and 16), the stable lines' size of groups I and III solutions decrease, on the other hand, the stable lines' size of group II solutions increases. Another case is when v is constant (*e.g.*, $v = 1.5$, Fig. 14) and H_3 varies, the stable lines' size of groups I and III solutions increase, on the other hand, the two stable lines of group II solutions became one from $H_3 = 0.1$ to $H_3 = 2$, and vanish at $H_3 = 10$. It is also important to mention that Saryshev and Mirer (2001), Sarychev et al. (2008) have made a similar study, but addressing the case where $H_2 = 0$, aligned with one of the principal planes of inertia. The objective in making $H_1 = 0$ is to address a different case not addressed by Saryshev and Mirer (2001), Sarychev et al. (2008), as well as to study the stability of small equilibrium regions addressed by Santos and Melicio (2020) which might lead to interesting academic results regarding the study and analysis of the general case (Santos and Melicio, 2020).

5. Conclusions

The objective of this work was the study of small equilibrium regions out of their main region when the vector of gyrostatic moment is tangent to the orbital plane. This objective is aligned to verify the results discovered in the general case presented by Santos (2015), which were confirmed and validated from the analysis of Figs. 7–9.

A mathematical analytical–numerical method was used to determine all equilibrium positions, the conditions of their existence and the sufficient conditions of stability. Three groups of equilibrium solutions were found: groups I, II, and III, each one describing up to eight equilibrium positions, totalising 24 maximum equilibrium positions. The direction cosines expressions are presented in the explicit form as a function of system dimensionless parameters v, H_2 and H_3. The bifurcation curves of group I and III solutions were determined analytically, and the equilibrium existence conditions of group II solutions were obtained as a function of parameters v, H_2 and H_3. A detailed evolution study of the gyrostat satellite equilibria bifurcation and an evolution study of the sufficient stability conditions validity for each equilibrium were conducted by a numerical-analytical method as a function of the system parameters v, H_2 and H_3. It was shown that there is no less than 8 and no more than 24 equilibrium positions for every studied case, more specifically, no less than 4 and more than 8 equilibrium positions for each group of solutions I, II, and III. The existence of small equilibria regions close to $H_1 = 0$ was confirmed.

Regarding the gyrostat stability, there is a minimum of two stable equilibrium positions for each studied case and a maximum of six stable equilibrium positions.

Declaration of Competing Interest

The authors declare that they have no known competing financial interests or personal relationships that could have appeared to influence the work reported in this paper.

Acknowledgments

The present work was performed under the scope of activities at the Aeronautics and Astronautics Research Centre (AEROG) of the Laboratório Associado em Energia, Transportes e Aeronáutica (LAETA), and was supported by the Fundação para a Ciência e Tecnologia by Project No. UIDB/50022/2020; by FCT, through IDMEC, under LAETA, project UIDB/50022/2020; FCT through ICT (Institute of Earth Sciences) project UIDB/04683/2020.

References

Aleksandrov, A.Y., Aleksandrova, E.B., Tikhonov, A.A., 2018. Stabilization of a programmed rotation mode for a satellite with electrodynamic attitude control system. Adv. Space Res. 62 (1), 142–151. https://doi.org/10.1016/j.asr.2018.04.006.

Anchev, A.A., 1973. Equilibrium attitude transitions of a three-rotor gyrostat in a circular orbit. AIAA J. 11 (4), 467–472. https://doi.org/10.2514/3.6775.

Chaikin, S.V., 2013. Bifurcations of the relative equilibria of a gyrostat satellite for a special case of the alignment of its gyrostatic moment. J. Appl. Math. Mech. 77 (5), 477–485. https://doi.org/10.1016/j.jappmathmech.2013.12.003.

Gorr, G.V., 2021. An approach in studying gyrostat motion with variable gyrostatic moment. Vestnik Udmurtskogo Universiteta. Matematika. Mekhanika. Komp'yuternye Nauki 31 (1), 102–115. https://doi.org/10.35634/vm210108.

Guirao, J.L.G., Vera, J.A., 2010. Dynamics of a gyrostat on cylindrical and inclined Eulerian equilibria in the three-body problem. Acta Astronaut. 66 (3–4), 595–604. https://doi.org/10.1016/j.actaastro.2009.07.024.

Gutnik, S.A., Santos, L., Sarychev, V.A., Silva, A., 2015. Dynamics of a gyrostat satellite subjected to the action of gravity moment. equilibrium attitudes and their stability. Journal of Computer and Systems Sciences International 54 (3), 469–482. https://doi.org/10.1134/s1064230715030107.

Gutnik, S.A.,Sarychev, V.A., 2013. Symbolic-Numerical Investigation of Gyrostat Satellite Dynamics. In: Computer Algebra in Scientific Computing. Springer International Publishing, pp. 169–178. doi:10.1007/978-3-319-02297-0_15.

Gutnik, S.A., Sarychev, V.A., 2014. Symbolic-numerical methods of studying equilibrium positions of a gyrostat satellite. Programming and Computer Software 40 (3), 143–150. https://doi.org/10.1134/s0361768814030049.

Gutnik, S.A., Sarychev, V.A., 2017. Application of computer algebra methods for investigation of stationary motions of a gyrostat satellite. Programming and Computer Software 43 (2), 90–97. https://doi.org/10.1134/s0361768817020050.

Kane, T.R., Ben-Asher, D.A.L.J.Z., 1983. Space Dynamics. chapter Simple Spacecraft. McGraw-Hill, pp. 159–246.

Kuang, J., Tan, S., 2002. GPS-based attitude determination of gyrostat satellite by quaternion estimation algorithms. Acta Astronaut. 51 (11), 743–759. https://doi.org/10.1016/s0094-5765(02)00031-0.

Li, T., Longman, R.W., 1982. Stability relationships between gyrostats with free, constant-speed, and speed-controlled rotors. Journal of Guidance, Control, and Dynamics 5 (6), 545–552. https://doi.org/10.2514/3.19787.

Longman, R.W., 1968a. The equilibria of orbiting gyrostats with internal angular momenta along principal axes. In: Proc. of the Symposium on Gravity Gradient Attitude Stabilization. El Segundo, California, USA. Published as 359 Air Force SAMSO-TR-69-307 (Aerospace Corporation Report No. TR-0066(5143)-1), pp. 3–53.

Longman, R.W., 1968b. Generalized approach to gravity-gradient stabilization of gyrostat satellites. Ph.D. thesis University of California San Diego, USA.

Longman, R.W., 1971. Gravity-gradient stabilization of gyrostat satellites with rotor axes in principal planes. Celestial Mechanics 3 (2), 169–188. https://doi.org/10.1007/bf01228031.

Longman, R.W., 1972. Stability Analysis of All Possible Equilibria for Gyrostat Satellities under Gravitational Torques. AIAA Journal 10 (6), 800–806. https://doi.org/10.2514/3.50214.

Longman, R.W., 1973. Stable tumbling motions of a dual-spin satellite subject to gravitational torques. AIAA Journal 11 (7), 916–921. https://doi.org/10.2514/3.6853.

Longman, R.W., 1975. Attitude equilibria and stability of arbitrary gyrostat satellites under gravitational torques. Journal of374 the British Interplanetary Society 28, 38–46, URL: https://ui.adsabs.harvard.edu/abs/1975JBIS...28...38L.

Longman, R.W., Roberson, R.E., 1969. General solution for the equilibria of orbiting gyrostats subject to gravitational torques. The Journal of the Astronautical Sciences 16 (2), 49–58.

Molina, R., Mondéjar, F., 2004. Equilibria and stability for a gyrostat satellite in circular orbit. Acta Astronaut. 54 (2), 77–82. https://doi.org/10.1016/s0094-5765(02)00282-5.

Nazari, M., Butcher, E.A., 2014. On the stability and bifurcation analysis of dual-spin spacecraft. Acta Astronaut. 93, 162–175. https://doi.org/10.1016/j.actaastro.2013.07.010.

Ousaloo, H.S., 2016. Active nutation control of an asymmetric spacecraft using an axial reaction wheel. Adv. Space Res. 58 (11), 2287–2303. https://doi.org/10.1016/j.asr.2016.07.034.

Pascal, M., Stepanov, S.I., 1991. On a semi-inverse problem in the motion of gyrostat satellites. Celestial Mechanics and Dynamical Astronomy 50 (2), 99–108. https://doi.org/10.1007/bf00051044.

Rubanovskii, V.M., 1991. Bifurcation and stability of the relative equilibria of a gyrostat satellite. J. Appl. Math. Mech. 55 (4), 450–455. https://doi.org/10.1016/0021-8928(91)90005-f.

Santos, L.F.F.M., 2015. Gyrostat dynamics on a circular orbit. Ph.D. thesis Universidade da Beira Interior Covilha, Portugal. doi:10400.6/4034.

Santos, L.F.M.M., Melicio, R., 2020. Bifurcation of equilibria for general case of gyrostat satellite on a circular orbit. Aerosp. Sci. Technol. 105, 106058. https://doi.org/10.1016/j.ast.2020.106058.

Sarychev, V.A., Gutnik, S.A., Silva, A., Santos, L.F.F.M., 2012. Dynamics of gyrostat satellite subject to gravitational torque. investigation of equilibria. Keldysh Institute of Applied Mathematics 63, 1–35.

Sarychev, V.A., Gutnik, S.A., Silva, A.R.R., Santos, L.F.F.M., 2013. Dynamics of gyrostat satellite subject to gravitational398 torque. stability analysis. Keldysh Institute of Applied Mathematics 25, 1–36.

Sarychev, V.A., Mirer, S.A., Degtyarev, A.A., 2005. The Dynamics of a Satellite-Gyrostat with a Single Nonzero Component of the Vector of Gyrostatic Moment. Cosm. Res. 43 (4), 268–279. https://doi.org/10.1007/s10604-005-0045-1.

Sarychev, V.A., Mirer, S.A., Degtyarev, A.A., 2008. Dynamics of a gyrostat satellite with the vector of gyrostatic moment in the principal plane of inertia. Cosm. Res. 46 (1), 60–73. https://doi.org/10.1134/s0010952508010085.

Saryshev, V.A., Mirer, S.A., 2001. Relative Equilibria of a Gyrostat Satellite with Internal Angular Momentum Along a Principal Axis. Acta Astronaut. 49 (11), 641–644. https://doi.org/10.1016/s0094-5765(01)00083-2.

Seo, I.-H., Leeghim, H., Bang, H., 2008. Nonlinear momentum transfer control of a gyrostat with a discrete damper using neural networks. Acta Astronaut. 62 (6–7), 357–373. https://doi.org/10.1016/j.actaastro.2008.01.014.

Shirazi, K.H., Ghaffari-Saadat, M.H., 2005. Bifurcation and Chaos in an Apparent-Type Gyrostat Satellite. Nonlinear Dyn. 39 (3), 259–274. https://doi.org/10.1007/s11071-005-3049-8.

Vera, J.A., 2009. Eulerian equilibria of a triaxial gyrostat in the three-body problem: Rotational Poisson dynamics in Eulerian equilibria with oblateness. Acta Astronaut. 65 (5–6), 755–765. https://doi.org/10.1016/j.actaastro.2009.03.014.

Wang, Y., Xu, S., 2012. Symmetry, reduction and relative equilibria of a rigid body in the J2 problem. Adv. Space Res. 51 (7), 1096–1109. https://doi.org/10.1016/j.asr.2012.10.030.

Zanardi, M.C., Moreira, L.S., 2007. Analytical attitude propagation with non-singular variables and gravity gradient torque for spin stabilized satellite. Adv. Space Res. 40 (1), 11–17. https://doi.org/10.1016/j.asr.2007.04.047.